Making the case for an alternate LBNF neutrino beam line.

nuPIL WG and DUNE LBWG
Fermi National Accelerator Laboratory,
Box 500, Batavia, IL 60510-5011, USA

(Dated: July 20, 2016)

Abstract

This note describes an alternate design (nuPIL) for the LBNF neutrino beam line. In order to make an informed decision whether or not to pursue this approach, the physics case first has to be made. In this note, we review the basic science requirements, give a brief description of the nuPIL concept and will show initial comparisons for CP sensitivity. We then will enumerate the minimum full set of physics analyses required to evaluate the overall performance of the LBNF/DUNE physics program for the case of the optimized LBNF conventional neutrino beam versus the neutrino beam available from a nuPIL configuration. The comparisons assume the same proton power on target and the same near and far detectors.

I. INTRODUCTION

In order to make a decision regarding whether or not to proceed with a detailed cost-benefit analysis of a neutrinos from a pion beam line (nuPIL) neutrino beam for LBNF, vs. the current configuration for the beam, a comparison of the physics performance of the DUNE suite of detectors using the current best estimate for the neutrino fluxes available in the two configurations must be completed in time for the DUNE collaboration meeting in May. This document will outline the first set of comparisons based on the LBNF 80 GeV optimized beam line design and nuPIL lattice 11 design with only the bend (no beam line elements in the straight/decay pipe). A full set of comparisons will then need to be made in order to make a comprehensive presentation to the DUNE collaboration. It is hoped that these analyses plus a preliminary cost-differential analysis will allow the collaboration to make an informed decision regarding a recommendation to the LBNF project office to proceed with the detailed cost-benefit analysis.

II. BASIC REQUIREMENTS

Any change to the LBNF neutrino beam requirements is undesirable. Therefore the nuPIL design must meet the LBNF global science requirements for the beam line:

1. The neutrino beam spectrum shall cover the energy region of the first two oscillation maxima affected by muon-neutrino conversion from the atmospheric parameters. For a baseline of 1300 km, with the current knowledge of parameters, the first two nodes are expected to be approximately 2.4 and 0.8 GeV. The matter effects dominate over the CP effects above 3 GeV and the CP effect dominates below 1.5 GeV. Adequate number of electron neutrino events with good energy resolution will allow DUNE to exploit this spectral information to determine mass hierarchy, CP phase, and a precise value of θ_{13} unambiguously. The beam spectrum will also allow muon disappearance measurement with two nodes. The nuPIL design can provide tuning capabilities in order to cover both maxima. The physics comparisons can include a nuPIL running scenario where the running is split between two energy tunes with the total exposure equal to that in the conventional LBNF beam line case.

2. The beam shall be sign-selected to provide separate neutrino and anti-neutrino beams with high purity to enable measurement of CP violation mass hierarchy, and precision oscillation measurement.

3. The electron neutrino content in the beam shall be kept small so that the systematic errors on the additional background has a small impact on the CP phase measurement (compared to the statistical error).

4. The neutrino beam spectrum shall extend beyond the first maximum to higher energies, while maintaining a high signal to background ratio to obtain the maximum number of charged current signal events. This will allow precision probes of the PMNS parameters that govern neutrino oscillations.

5. The beam shall be aimed at the far detector with an angular accuracy that allows the determination of the far detector spectrum using the near detector measurements. The angular accuracy shall not be the dominant factor in the determination of oscillation parameters.

6. The beam shall be capable of operating with a single-turn, fast-extracted primary proton beam from the Main Injector with greater than 2 MW of power. The fast extraction enables short spills which are essential for good cosmic ray background rejection for detectors.

7. The beam line shall be able to accept a range of Main Injector proton energies that is well matched to the oscillation physics requirements. Proton beam energies of around 60 GeV are optimal for the simultaneous measurements of CP violation and MH, while higher energy beams (the maximum possible from the Main Injector is 150 GeV) can probe physics beyond the 3-flavor mixing, and probe tau-appearance with higher statistics.

In addition, the basic physics requirements are:

1. For CP 3 σ sensitivity over 75% of the δ_{CP} range with an 850 kt*MW*yr exposure.

2. Resolution on δ_{CP} of better than 20 degrees.

3. Precision measurement of all oscillation parameters including θ_{13}.

III. NEUTRINO FLUXES FOR INITIAL STUDY

In order to provide a first physics comparison for the DUNE collaboration meeting in May, nuPIL lattice 11 was chosen as the baseline for the bend with no beam line elements in the straight (decay pipe). Lattice 11 was optimized for this (decay pipe) configuration. A 4 m diameter by 204 m long decay pipe is assumed, as is the case in the baseline LBNF design. Work continues on matching the bend to the straight beam line elements (the preferred implementation, we believe) and a complete (horn to decay straight end) nuPIL bean line configuration should be available for study shortly after the DUNE collaboration meeting.

A. nuPIL lattice 11

The basic concept for the nuPIL beam line design is an outgrowth of the nuSTORM pion beam line [1, 2]. Concepts for nuPIL have gone through 13 lattice designs to date. We have chosen lattice 11 for this study. Lattice 11 is an achromatic beam line composed of a dispersion creator and two bending matching cells, made of scaling FFAG magnets as shown in Figure 1. There are 10 elements in the bend with the trajectory dropping 2 m from the downstream end of the horn. Table I gives the parameters of the magnets in the bend and Table II gives the lattice description.

Table I. Parameters of the magnets.

Magnet	Number of	Excursion	Length	Gap size	B_{max}	B_{min}	L_{coil}
type	magnets	[m]	[m]	[m]	[T]	[T]	[m]
F1	4	0.82	2.6	0.66	1.48	0.11	7.5
D1	2	0.72	4.0	0.66	1.29	0.13	10
F5	1	0.92	4.6	0.66	0.50	0.12	11.5
D3	1	0.84	3.3	0.66	0.52	0.14	9
D4	1	0.87	1.6	0.66	1.64	0.41	5.5
F5	1	0.80	2.2	0.66	1.35	0.38	6.5

Figure 2 shows the evolution of the transmitted pion momentum distribution from the downstream face of the horn to the end of the bend and Figure 3 shows representative particle trajectories through the bend.

Table II. Lattice parameters of the nuPIL FFAG bend.

Dispersion creator	FDF triplet ×2
radius (5 GeV/c)	386.3
k-value	1240
periodic dispersion [m]	0.31
final dispersion [m]	0.62
opening angle [deg]	1.7 ×2
final excursion (3-10 GeV/c) [m]	0.75
length [m]	23
phase advance (H/V) [deg]	(65, 187)
max magnetic field [T]	1.5
Bending cell 1	FD doublet
radius (5 GeV/c)	541.2
k-value	867.8
opening angle [deg]	1.2
periodic dispersion [m]	0.62
length [m]	11
Final beta [m] (5 GeV/c) (H/V)	(8.4, 48.1)
max magnetic field [T]	0.6
Bending cell 2	DF doublet
radius (5 GeV/c)	255.0
k-value	408.4
opening angle [deg]	1.2
periodic dispersion [m]	0.62
length [m]	5
Final beta [m] (5 GeV/c) (H/V)	(26.6, 24.1)
max magnetic field [T]	1.5

B. Neutrino flux

The nuPIL fluxes have been calculated using a nuSTORM horn with a 38 cm long (2.5 interaction length) Inconel target. Optimization of the target/horn module for the nuPIL lattice has not yet been done, but will start soon. Production off the target and through the horn (nuSTORM baseline which was "NuMI-like") was simulated with MARS15 using realistic horn material parameters. This parent particle distribution (pions, Kaons and protons) at the downstream face of the horn was tracked through the bend using the Lagrange code, which has been cross-checked against Zgoubi [3] and bench-marked by experiment [4]. All

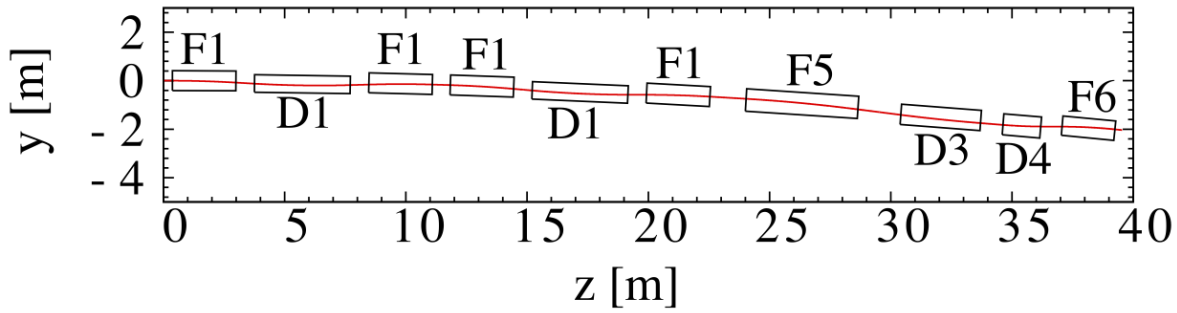

Figure 1. Layout of the nuPIL bend (lattice 11) with the magnet types labeled. The black lines show the effective field boundaries of the magnets.

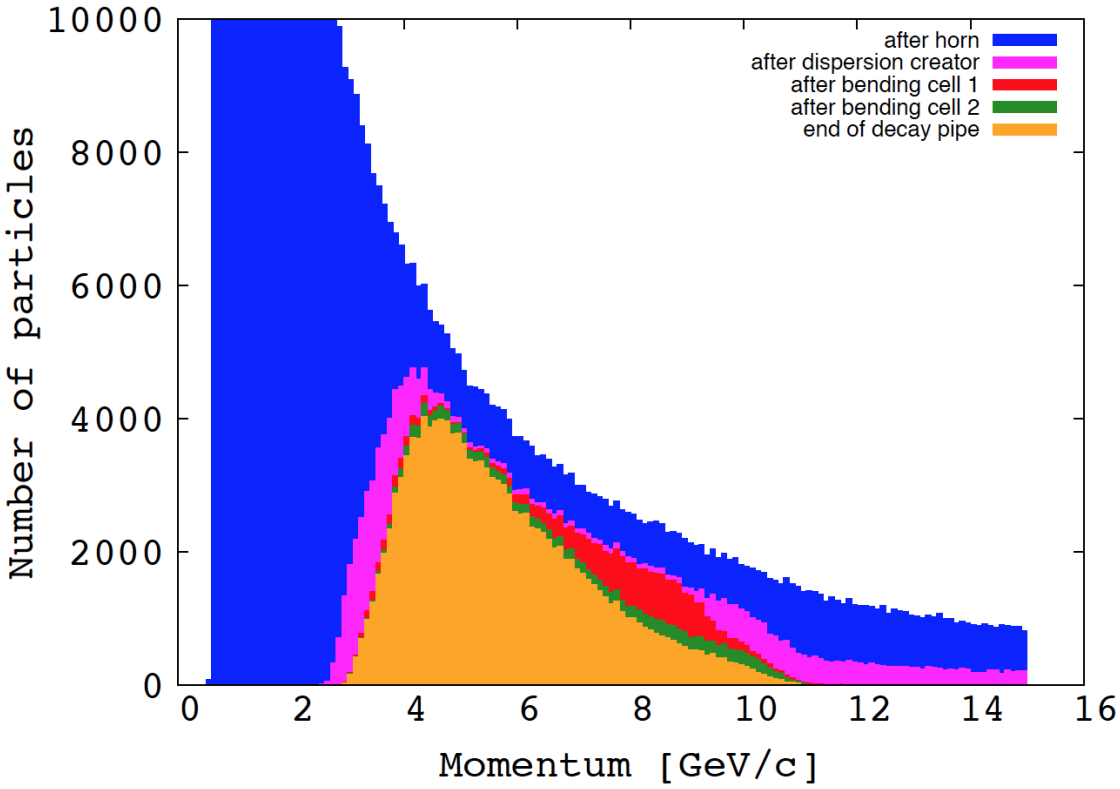

Figure 2. Momentum distribution of transmitted pions along the FFAG bend. In the simulation done to produce this plot, pion decay has been turned off. Note that the difference between the distribution at the end of the bend and at the end of the decay pipe is very small. Lattice 11 comes close to ideal collimation of the selected pions, since almost all of them reach the end of the decay pipe (do not hit the wall).

pions, kaons and protons exiting the horn and within the aperture of the first beam line element are tracked. For the neutrino beam, π^- and K^- are also tracked and vice versa for the anti-neutrino beam.

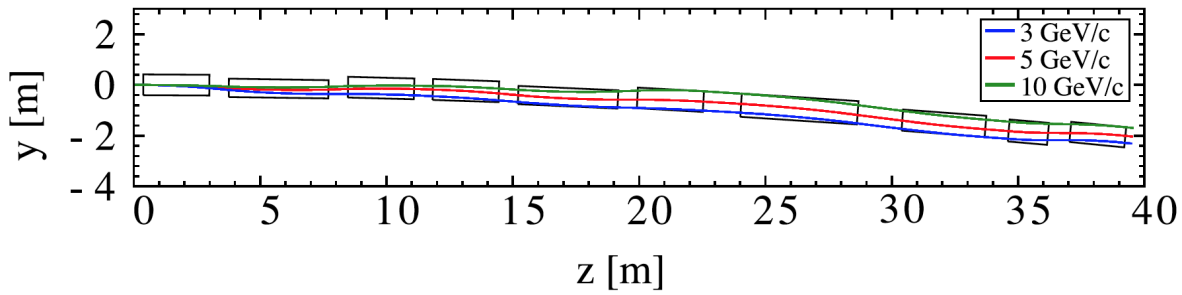

Figure 3. FFAG bend. Trajectories for 3, 5 and 10 GeV/c particles are shown.

1. Flux at the Far Detector

Figure 4 gives the neutrino beam ($\nu_\mu, \bar{\nu}_\mu$ and ν_e) for the LBNF 80 GeV optimized beam and for the nuPIL lattice 11 beam, based on particle distributions exiting the bend, as described in the preceding paragraph. The anti-neutrino beam is given in Figure 5.

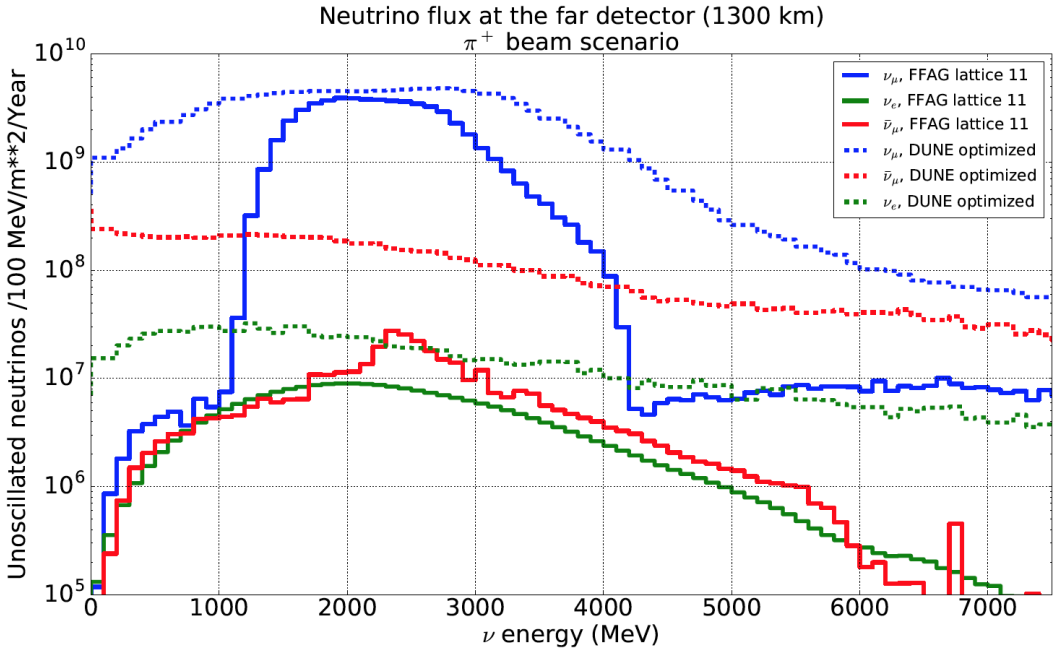

Figure 4. Neutrino fluxes for the optimized 80 GeV LBNF beam and the nuPIL beam (including all backgrounds.)

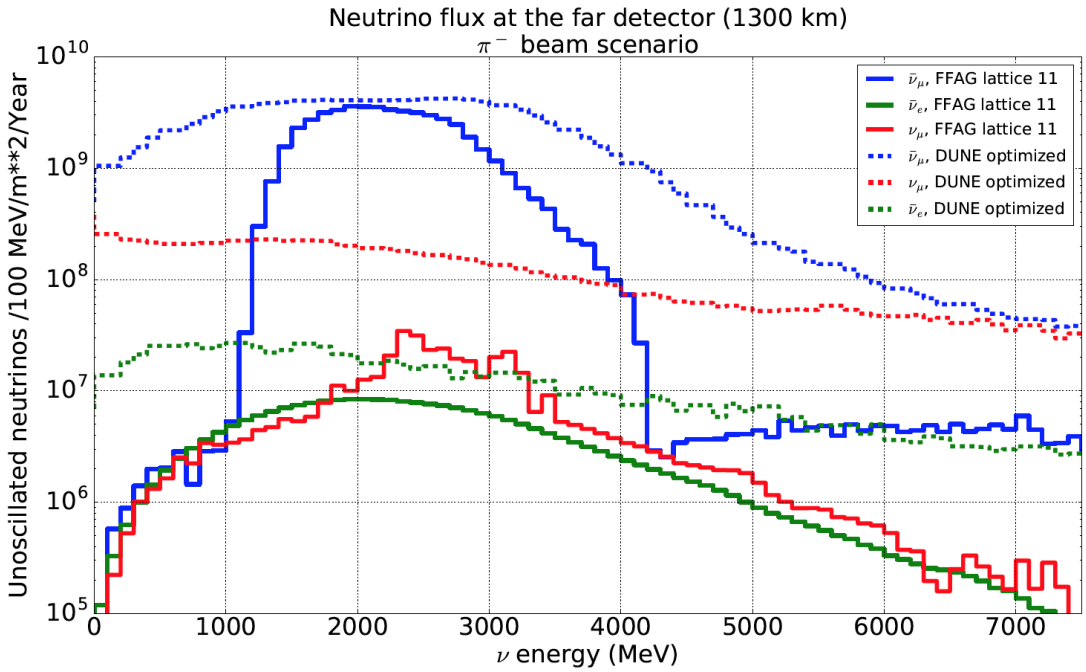

Figure 5. Anti-Neutrino fluxes for the optimized 80 GeV LBNF beam and the nuPIL beam (including all backgrounds.)

2. Flux at the Near Detector

In a nuPIL configuration for LBNF, the beam design allows for the near detector hall to be located much closer to the end of the decay straight due to the fact that there is no high-energy component (pions, muons or protons) in the beam. In the nuPIL configuration, the near detector hall can be located 50 m from the end of the straight. See Figure 6. This configuration yields a potential large cost savings in civil construction. The ND site neutrino and anti-neutrino fluxes at this distance from the end of the straight in the nuPIL configuration are given in Figures 7 and 8 respectively.

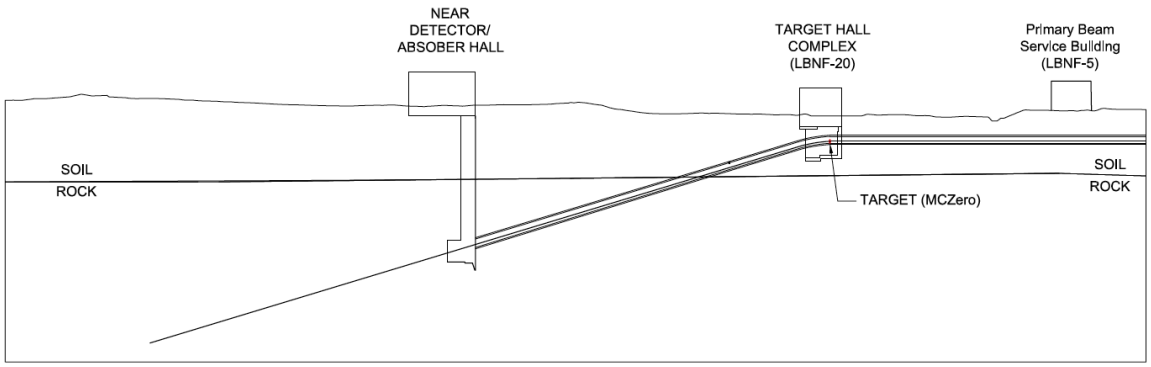

Figure 6. Near detector hall configuration for nuPIL.

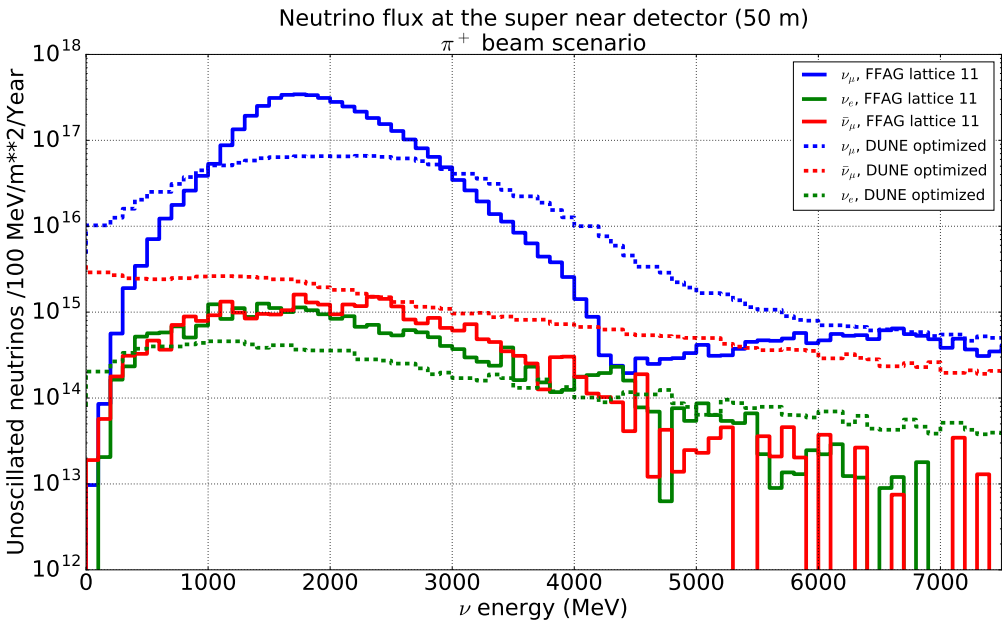

Figure 7. Neutrino flux at the nuPIL near hall site at a position 50 m from the end of the bend.

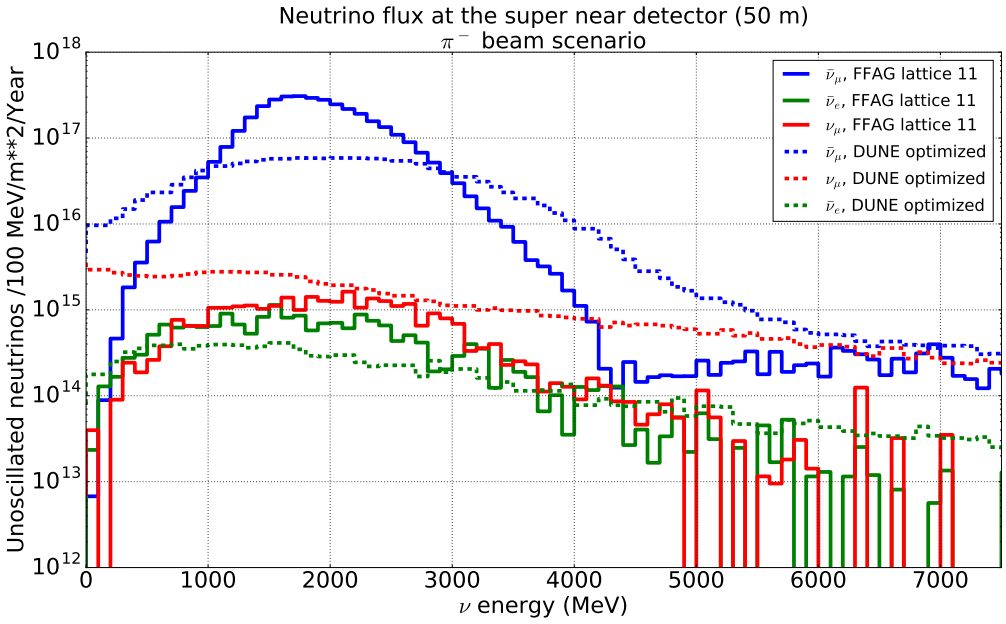

Figure 8. Anti-neutrino flux at the nuPIL near hall site at a position 50 m from the end of the bend.

C. Computing Sensitivities

In order to efficiently compare and benchmark NuPIL versus LBNF conventional, it was agreed to engage with the DUNE LBWG to compute sensitivities (to avoid the arguments if his sensitivity calculation is right or wrong). The LBWG, once provided with the fluxes (see above), will provide the standard benchmark plots i.e. CPV, MH, θ_{23} vs. δ_{CP}, θ_{13} vs. δ, etc. to be presented at the DUNE Collaboration meeting.

1. Sensitivity comparison - Pilar Coloma

Simulations done for the fluxes shown in Figures 4 and 5. Far detector configuration is assumed to be 40 kT of LAr and, of course, is the same for LBNF/DUNE and nuPIL/DUNE. Information from any near detectors has not been used. The oscillation parameters used for this analysis are:

1. θ_{23}=42 degree
2. θ_{13}=9 degree
3. θ_{12}=33 degree
4. $\Delta m^2_{atm} = 2.45 \times 10^{-3}$
5. $\Delta m^2_{sol} = 7.64 \times 10^{-5}$

Six years of running is assumed (3 in neutrino and 3 in anti-neutrino), 40kT and 1.1MW for a total exposure of $\simeq$250kT*MW*yr. The detector has been implemented using the following criteria:

- intrinsic ν_e and $\bar{\nu}_e$ contamination, with the same efficiency as the signal;
- neutral-current (NC) backgrounds coming from the leading flux component after interacting at the detector. Migration matrices are used to account for the mis-reconstruction at low energies. A rejection efficiency of 99.5% is assumed for the appearance channels, and 99% for disappearance.

- tau contamination backgrounds are implemented. The total number of CC ν_τ events is multiplied by the branching ratio of the τ for a leptonic decay (17%). A rejection efficiency of 40% is assumed. This gives a number of events that matches approximately the number of tau-induced events in the CDR. The migration to different energy bins is performed using migration matrices produced for liquid argon in Ref. [5]. The CC tau cross section is taken from Ref. [5] as well, which was produced using GENIE.

An overall normalization uncertainty was implemented for all signal and background contributions. This is bin-to-bin correlated. It is correlated among all contributions to the signal or background event rates in a given channel, but uncorrelated among different oscillation channels. Normalization uncertainties for the signal are set to 2% for appearance channels, and 5% for disappearance channels. Background uncertainties are set to 20% for appearance channels, and 10% for disappearance channels.

Unless otherwise stated, marginalization is performed over all oscillation parameters using the pull-method within the current experimental uncertainties on Δm^2_{31} , Δm^2_{21}, θ_{12}, $\sin^2 2\theta_{13}$ and $\sin^2 \theta_{23}$. In addition, degeneracies involving the octant of the atmospheric mixing angle and/or the neutrino mass ordering are fully searched for.

Figures 9 and 10 give the event rates for LBNF/DUNE and nuPIL/DUNE, respectively. For LBNF/DUNE there are 953 signal events and 221 background for the ν_e appearance channel and 210 signal and 165 background for the $\bar{\nu}_e$ channel. Figure 11 shows a comparison of the CP sensitivity as a function of δ. The CP fraction coverage as a function of exposure (1=250kT-MW-yr) is given in Figure 12. Finally, the sensitivity for the mass ordering is given in Figures 13 and 14 for normal and inverted hierarchy, respectively.

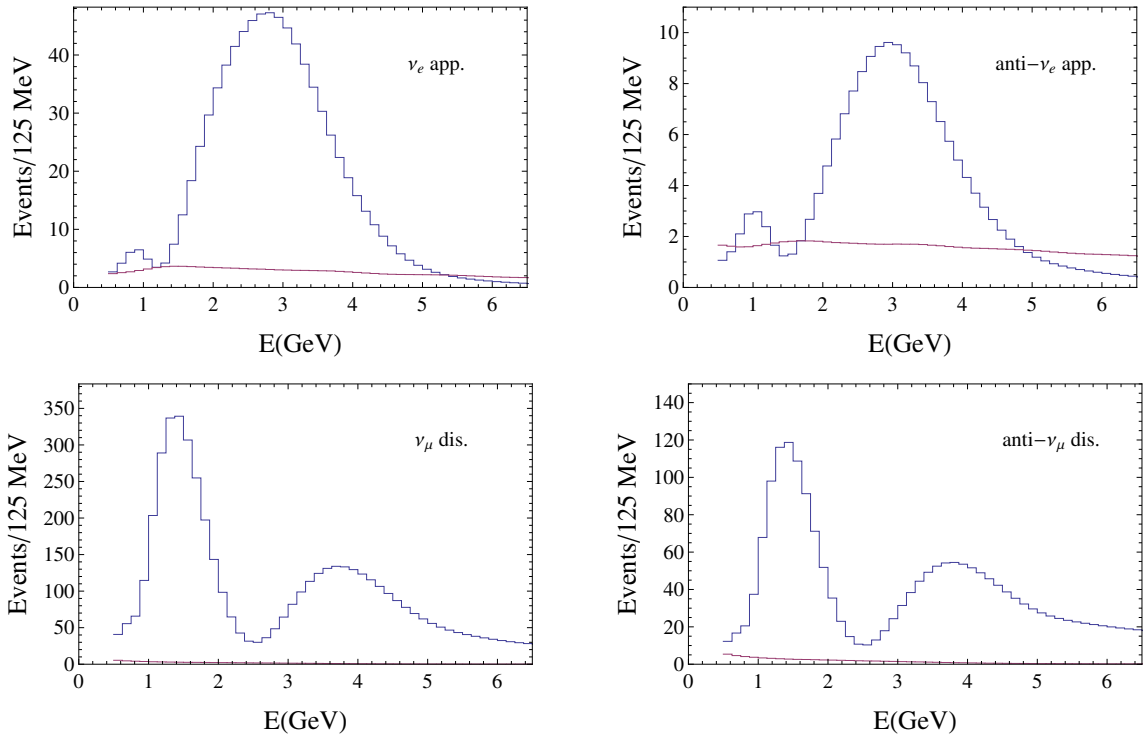

Figure 9. Events rates per bin for LBNF/DUNE, as a function of the neutrino energy in GeV. Blue (yellow) lines correspond to the total expected signal (background) rates. (Note that these are not stacked histograms.) The nominal exposure of 250 kt × MW × yr has been assumed.

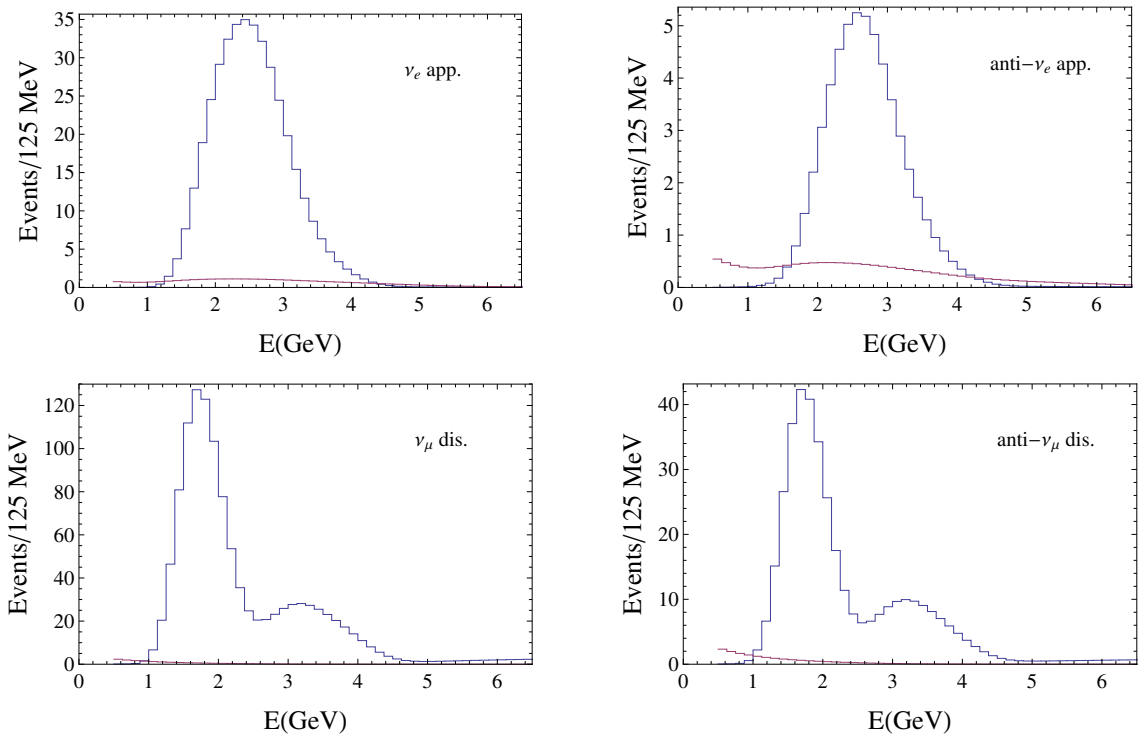

Figure 10. Events rates per bin for nuPIL/DUNE, as a function of the neutrino energy in GeV. Blue (yellow) lines correspond to the total expected signal (background) rates. (Note that these are not stacked histograms.) The nominal exposure of 250 kt × MW × yr has been assumed.

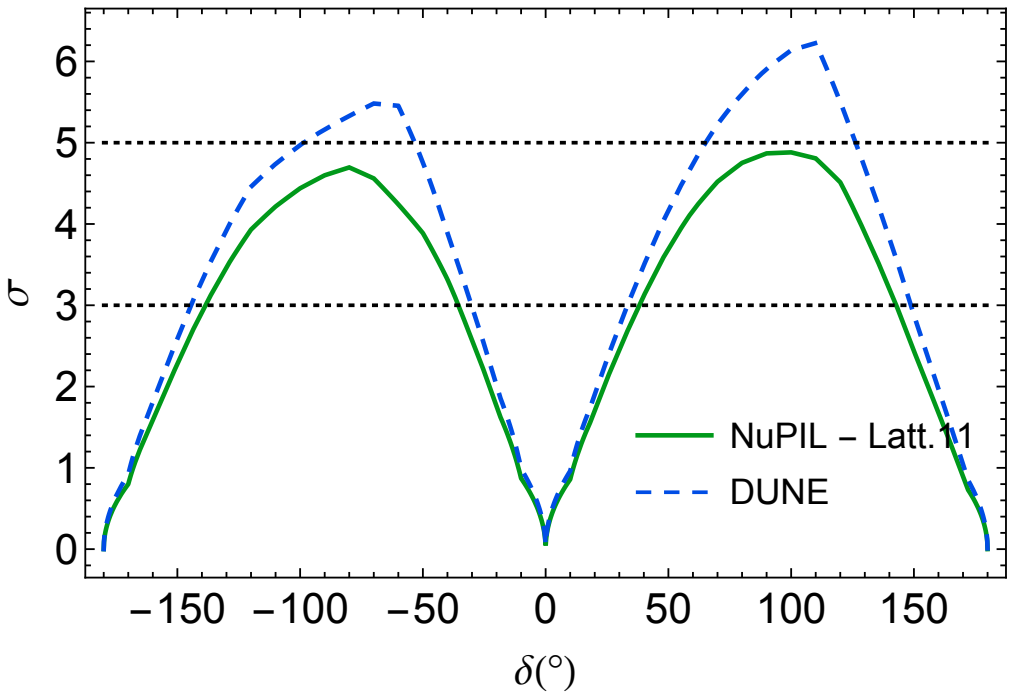

Figure 11. CP-violation sensitivity in number of sigmas, as a function of the true value of δ. Normal ordering is assumed, and nominal exposure is considered for both experiments.

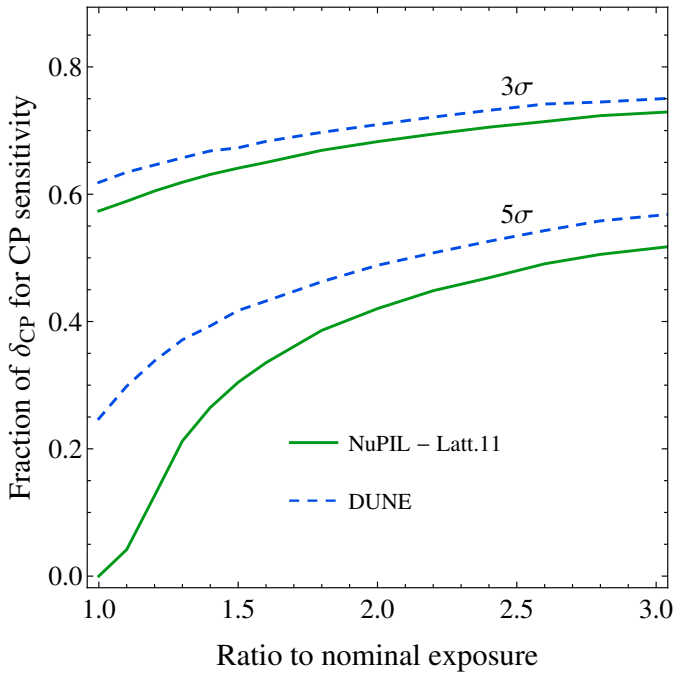

Figure 12. Fraction of possible true values of δ for which CP violation would be observed at 3σ (upper set of lines) and at 5σ (lower set of lines). Results are shown as a function of the ratio between the total exposure assumed with respect to the nominal exposure of 250kt $\times$ MW $\times$ yr.

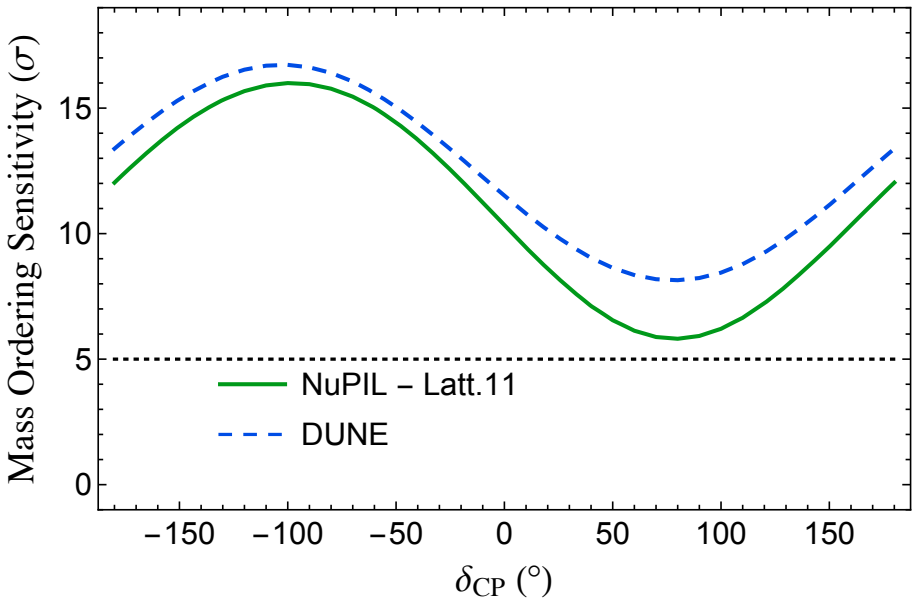

Figure 13. Sensitivity to the neutrino mass ordering, as a function of the assumed true value of δ, under the assumption of a true normal ordering ($\Delta m^2_{31} > 0$). Nominal exposure has been assumed.

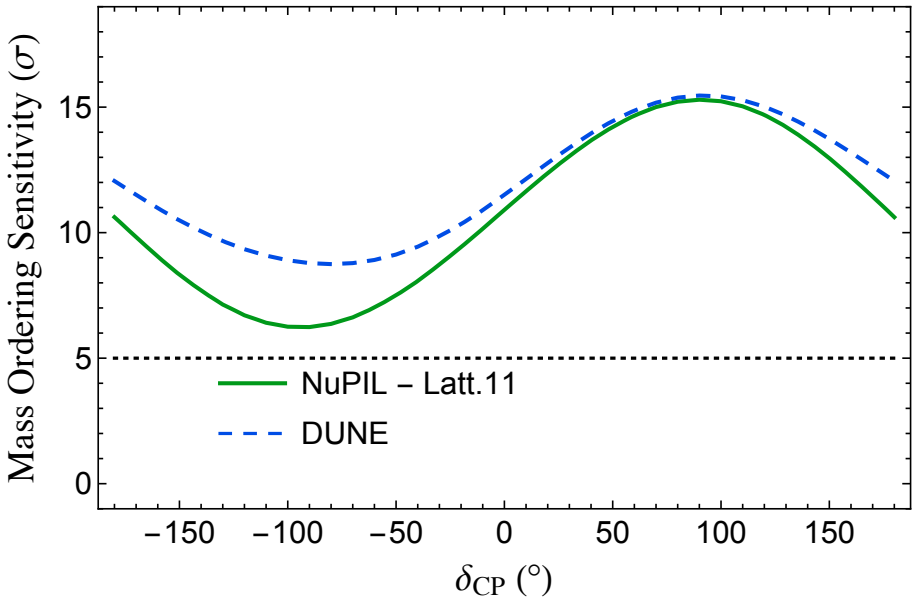

Figure 14. Same as Fig 10, under the assumption of a true inverted ordering ($\Delta m^2_{31} < 0$).

2. Sensitivity comparison - Elizabeth Worcester/Lisa Whitehead

Unless otherwise noted, all configurations (GLoBES code, oscillation parameters, systematic uncertainties, selection efficiencies, etc.) are identical to those used in the DUNE CDR. There are two LBNF fluxes used in this section. The first is "LBNF optimized" which is a flux derived from the CDR parameter set with the exception that the flux here uses a 204 m long decay pipe, whereas the CDR used a 250 m long decay pipe. The second is "LBNF 3-horn optimized" which is the updated LBNF design with 3 horns. The nuPIL flux is the "Lattice 11" design as used in the previous section.

Since each optimization prefers a different beam energy and the number of POT/year provided by the FNAL complex varies with beam energy, we must compare event rates and spectra assuming equal run time, corresponding to the following POT:

1. LBNF optimized: 80 GeV = 14.7×10^{20} POT/year.
2. LBNF 3 horn: 62 GeV = 18.3×10^{20} POT/year.
3. nuPIL: 120 GeV = 11.1×10^{20} POT/year.

As in the CDR, the spectra are stacked histograms, so that the "signal" histogram is the sum of all signal and background. The antineutrino component is plotted separately as a dashed histogram, so that the size of the wrong–sign contribution is visible. This is done for both FHC and RHC modes, but only the RHC mode has a significant wrong–sign component. Figures 15, 16 and 17 give the ν_e appearance spectra for the LBNF optimized, LBNF optimized 3-horn and nuPIL fluxes respectively. The sensitivity for the mass hierarchy and the CP phase are given in Figure 18 where curves for the two LBNF fluxes and the nuPIL flux are given. The curves shown in this figure assume and 7 years of running equally divided between neutrino and antineutrino. In Figure 19, we show the effect that systematic uncertainties have on the CP violation sensitivity. In order the enhance the effect, the exposure was increased to 20.8 years, again equally divided between neutrino and antineutrino running. The nominal systematic uncertainty (solid lines) assumes a 2% uncertainty for the appearance signal and 5% for the disappearance signal. Variations in the appearance normalization uncertainty were also considered. The broad-dotted curves correspond to a 1% appearance normalization uncertainty (keeping disappearance and background uncertainties

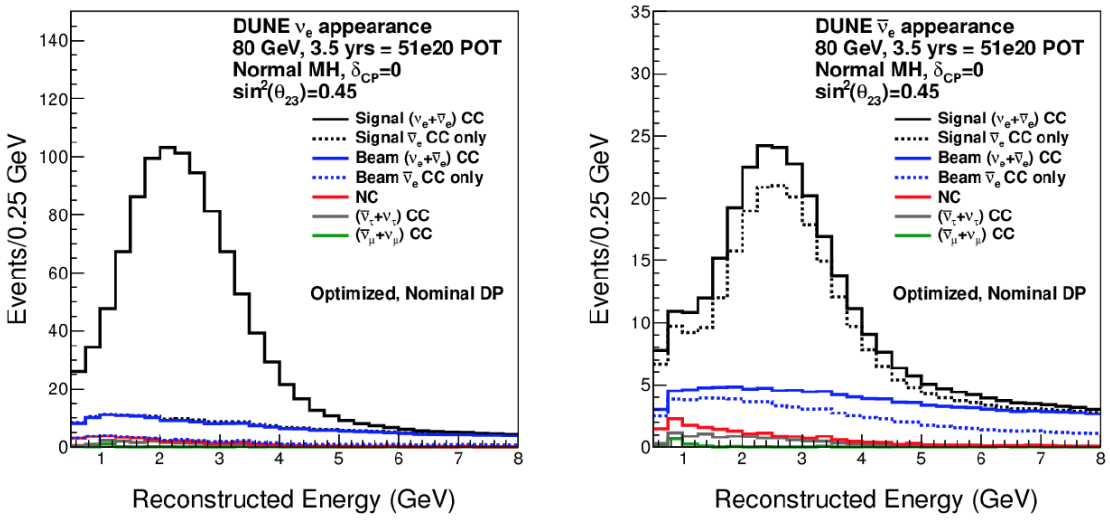

Figure 15. ν_e spectra for the LBNF Optimized (CDR) flux.

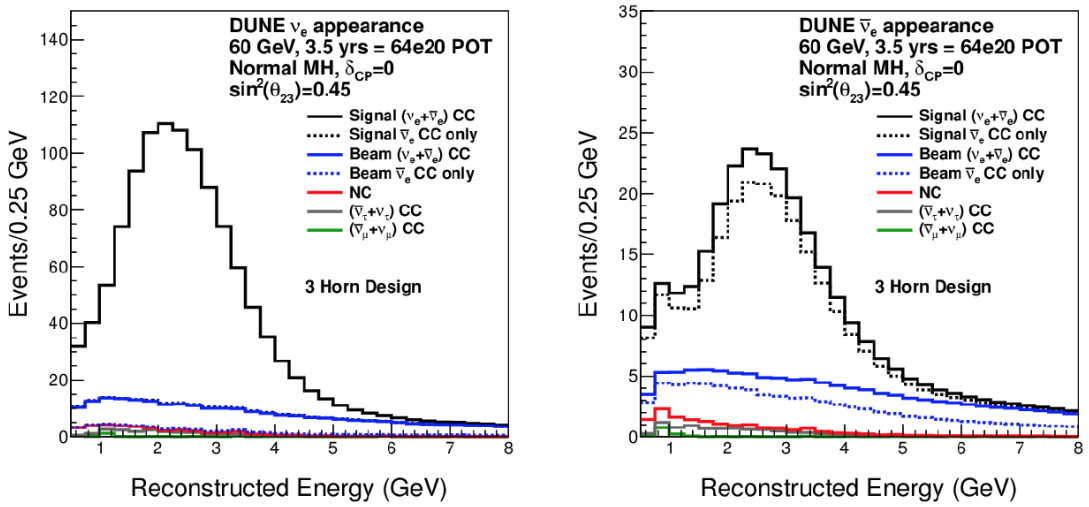

Figure 16. ν_e appearance spectra for the LBNF 3-horn Optimized flux.

unchanged) while the narrow-dotted curves correspond to a 5% appearance normalization uncertainty (again, keeping disappearance and background uncertainties unchanged). With this test, the conclusion regarding the relative strengths of the 3 fluxes remains unchanged. However, the figure does point to the large impact this type of systematic uncertainty could have on the experimental reach.

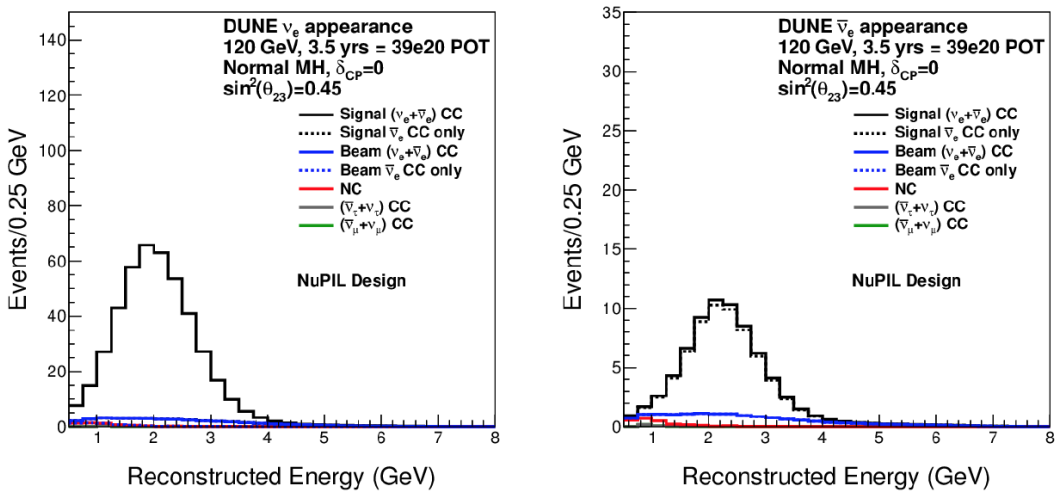

Figure 17. ν_e appearance spectra for the nuPIL flux.

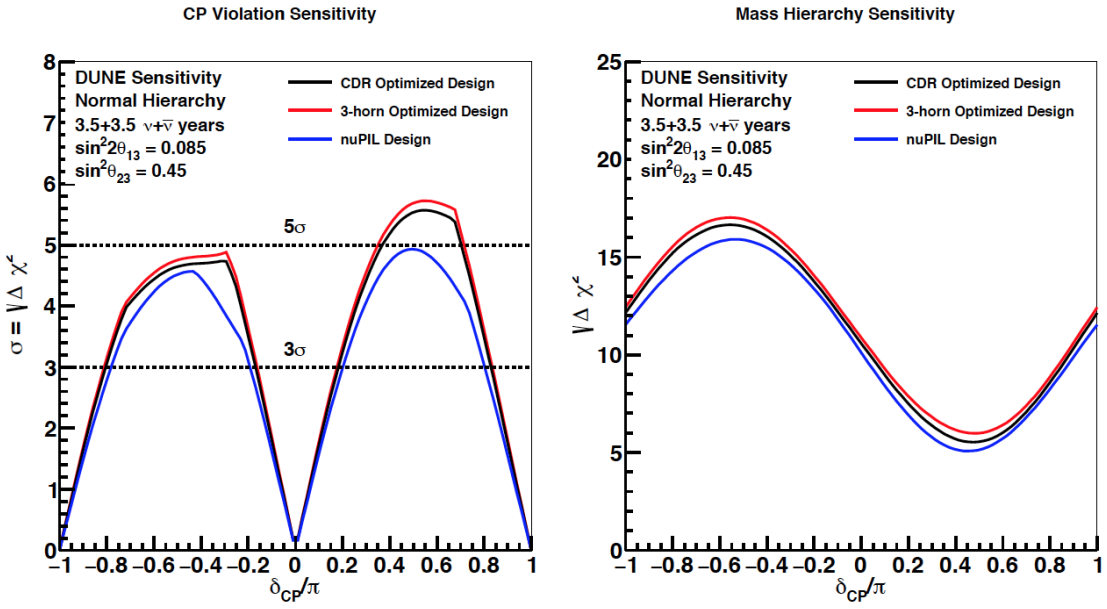

Figure 18. Sensitivity in the CP violating phase δ and the mass hierarchy for the two LBNF fluxes and the nuPIL flux.

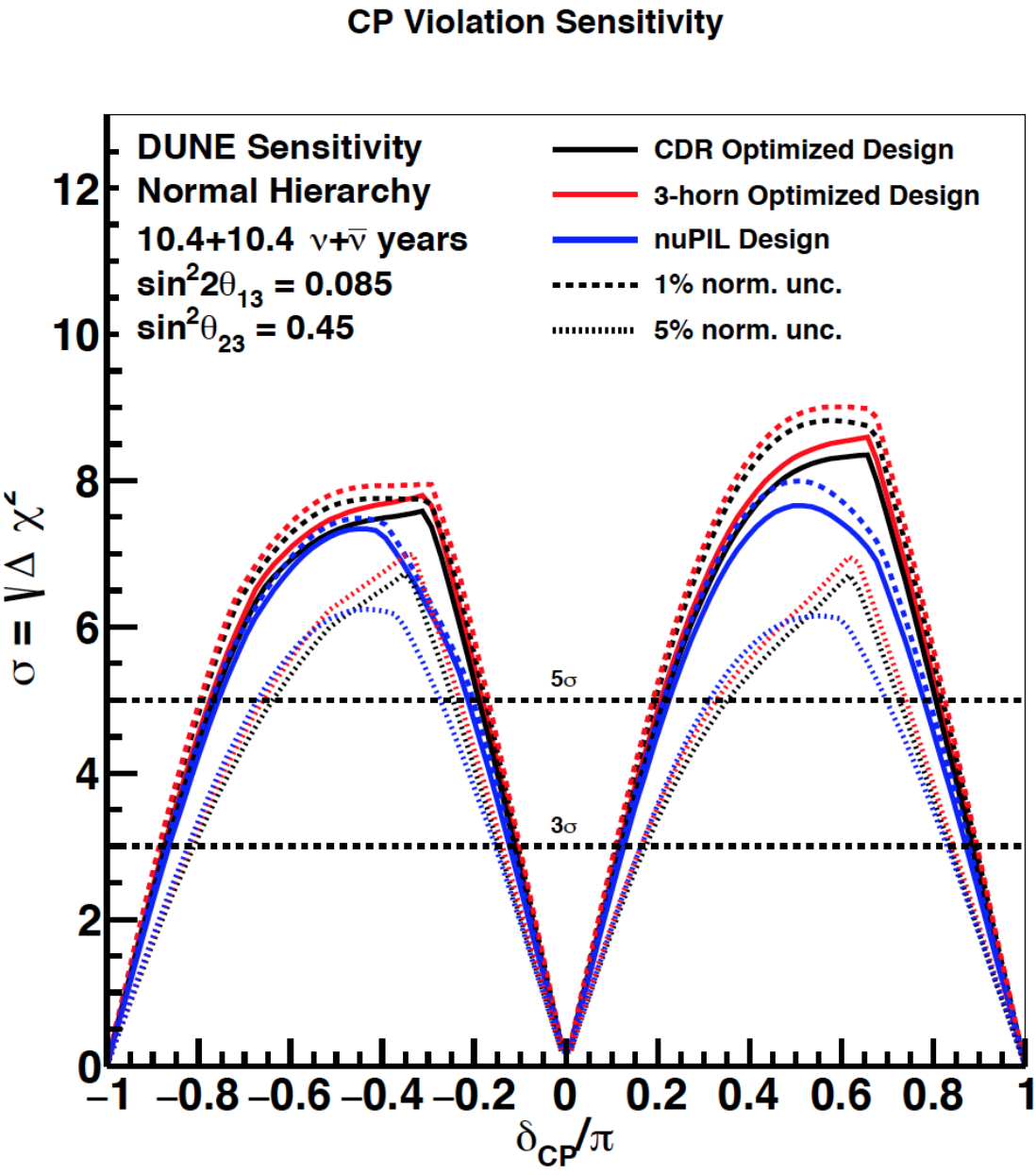

Figure 19. Demonstration of the impact that systematic uncertainties can have on experimental reach.

IV. NEUTRINO FLUX - SECOND STUDY

In this section we described an updated design for the nuPIL pion beam line and the neutrino fluxes that it produces. In this case, the physics comparisons to the conventional LBNF neutrino flux will use the new 3-horn optimized design with a NuMI-style target operating with the MI set at 62.5 GeV (1.83×10^{21}) protons on target per year. The new nuPIL configuration consists of a new design for the bend (Lattice 13) matched into a Quadrupole-channel beam line for the production straight.

A. Lattice 13 bend

A bending beam line composed of scaling FFAG magnets with a 5.8 deg. bend has been designed and its performance evaluated using Runge Kutta code. The layout of the FFAG bend is presented in Fig. 20. It is composed of a dispersion creator section and a dispersion suppressor section to transport a large momentum, and an optics matching section made of quadrupoles at the end of the bend to minimize the divergence of the beam at the entrance of the decay pipe. The parameters for these magnets is given in Table III.

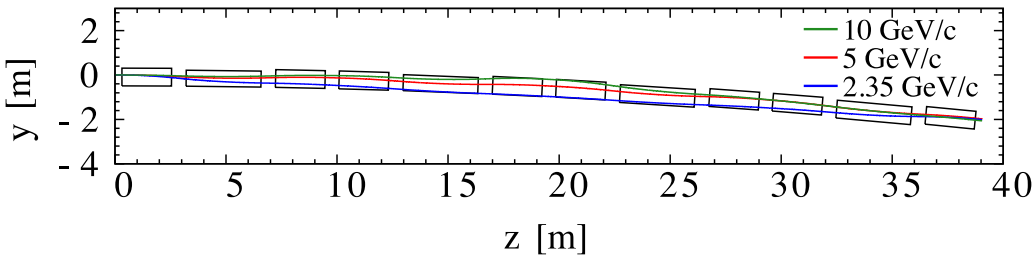

Figure 20. Beam line composed of scaling FFAG magnets with trajectories of 3 GeV/c, 5 GeV/c and 10 GeV/c. The horn is located at the $x = 0$ position, and the decay pipe starts at the end of the bend, at the $x = 39$ m position.

Table III. Parameters of the magnets.

Magnet type	Number of magnets	Excursion [m]	Length [m]	B_{max} [T]	B_{min} [T]
F	8	0.80	2.23	1.55	0.05
D	4	0.80	3.37	1.54	0.05

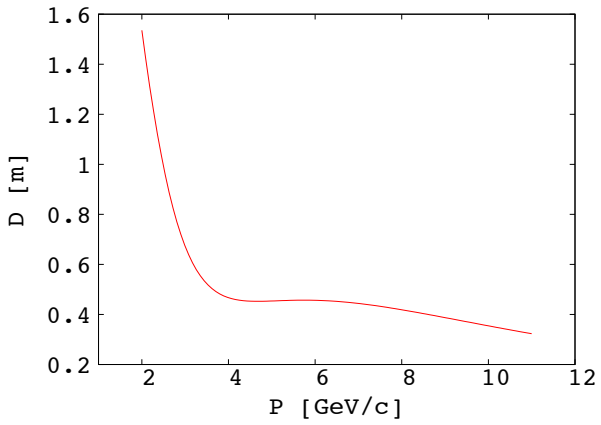

Figure 21. Dispersion value as a function of momentum at the exit of the dispersion creator.

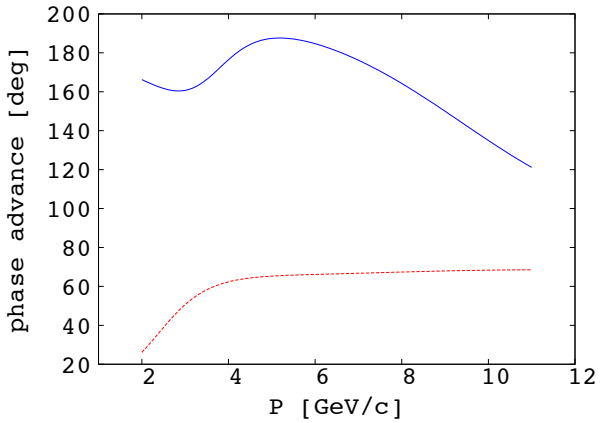

Figure 22. Phase advances in the bending plane (solid blue) and in the non-bending plane (dotted red) as a function of momentum at the exit of the dispersion creator.

1. Dispersion creator and suppressor

The dispersion creator principle in scaling FFAGs was recently developed [**?**]. The dispersion creator in the nuPIL case involves a very large momentum spread, and several dispersion creators in cascade would be necessary to create a proper dispersion for all momenta. To keep the bending beam line short, a single dispersion creator is used in the nuPIL design, with a phase advance higher than 180 deg. in the bending plane to accommodate a larger momentum spread. The dispersion and phase advances have been computed by tracking and the results are presented in Fig. 21 and 22.

Table IV. Lattice parameters of the nuPIL lattice 13-AA.

Dispersion creator/suppressor	FDF triplet ×4
radius (5 GeV/c)	386.5
k-value	1695
periodic dispersion [m]	0.228
final dispersion [m]	0.46
opening angle [deg]	1.45 ×4
Maximum excursion (2.35-10 GeV/c) [m]	0.8
length [m]	9.8
phase advance (H/V) [deg]	(65, 187)
periodic beta, alpha (bending plane at 5 GeV/c) [m,/]	(11.32, 0)
periodic beta, alpha (non-bending plane at 5 GeV/c) [m,/]	(11.32, 0)
max magnetic field [T]	1.5

2. Optics matching section

The matching section is designed to adjust the optics to a suitable value at the entrance of the decay pipe. The divergence needs to be minimised, so the Courant-Snyder parameter $\gamma = \frac{1+\alpha^2}{\beta}$ needs to be minimised in both planes. The α parameter should then be null, and the beta value as large as possible. This optics matching is done at the beginning of the decay channel, not discussed here.

3. Lattice parameters and performances

The parameters of the lattice 13-AA are summarised in Tab. IV. The dispersion function and beta functions have been computed around 5 GeV/c in tracking and can be seen in Fig. 23. The magnetic field for the maximum momentum is presented in Fig. 24, and shows that the magnets are within the normal conducting range.

The pion distribution coming out of the optimized horn has been tracked in the FFAG bend, and the surviving particles have been computed to estimate the resulting neutrino flux at the far detector and is presented in Fig. **??**. The momentum distribution of the pions after the horn and at the end of the bend are presented in Fig. 25.

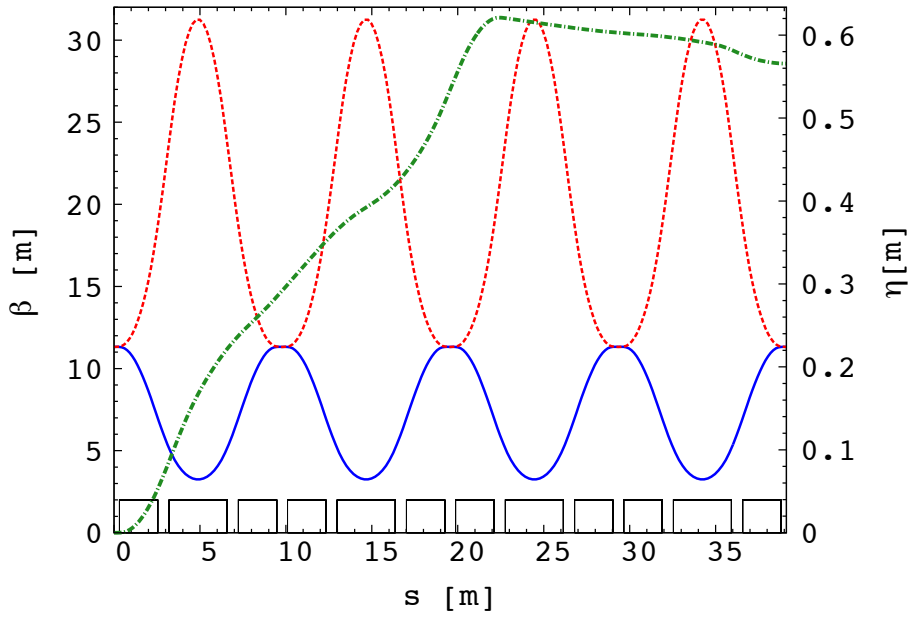

Figure 23. Beta functions in the bending plane (solid blue), in the non-bending plane (dotted red) and dispersion function (dot-dashed green) in the FFAG lattice 13 up to the decay channel at 5 GeV/c.

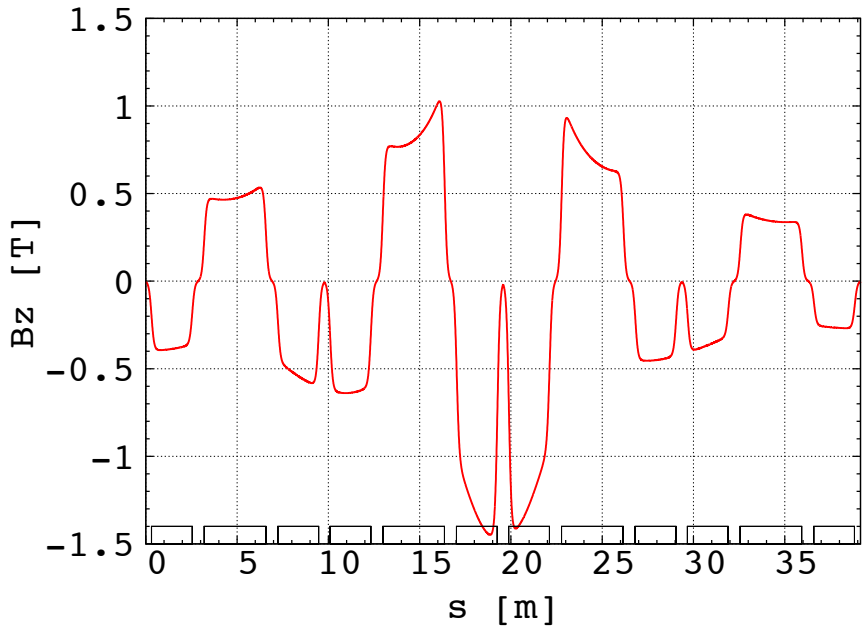

Figure 24. Magnetic field for 10 GeV/c pion reference trajectory in the FFAG bend.

B. Quadrupole beam line straight

After the FFAG bend, the beam (pions + protons + kaons) is matched into a quadrupole triplette (FDF) channel. Blah, Blah, Blah. Figure 26 show a G4Beamline visualization of the

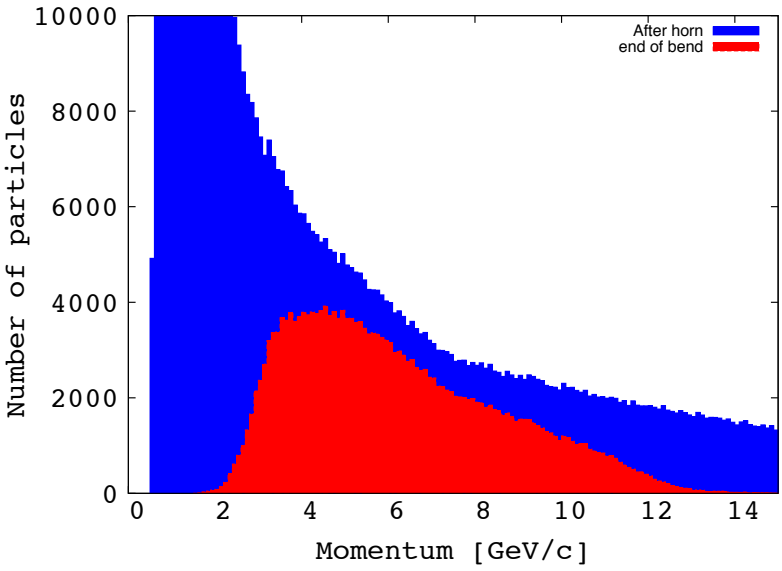

Figure 25. Momentum distribution of the pions from the optimized horn with a carbon target after the horn (blue) and at the end of the bend for nuPIL-Lattice13-AA.

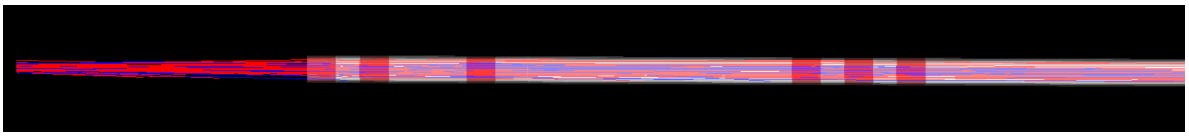

Figure 26. G4Beamline visualization of the matching section and one cell of the quad channel.

3 matching quads plus one cell. The red vertical bands represent the quadrupole magnets and the various colored horizontal lines represent particle trajectories. subsectionNeutrino flux The nuPIL fluxes have been calculated using a horn with a 160 cm long (4 interaction length) carbon target that has been optimized for the Lattice 13 input acceptance. Production off the target was simulated using MARS15. This parent particle distribution (pions, Kaons and protons) at the downstream face of the horn was tracked through the bend using the Lagrange code. All pions, kaons and protons exiting the horn and within the aperture of the first beam line element are tracked. For the neutrino beam, π^- and K^- are also tracked and vice versa for the anti-neutrino beam.

1. Flux at the Far Detector

Figure 27 gives the neutrino beam ($\nu_\mu, \bar{\nu}_\mu$ and ν_e) for the LBNF 62.5 GeV 3–horn optimized beam and for the nuPIL lattice 13-hybrid beam, based on particle distributions exiting the bend, as described in the preceding paragraph. The anti-neutrino beam is given in Figure 28.

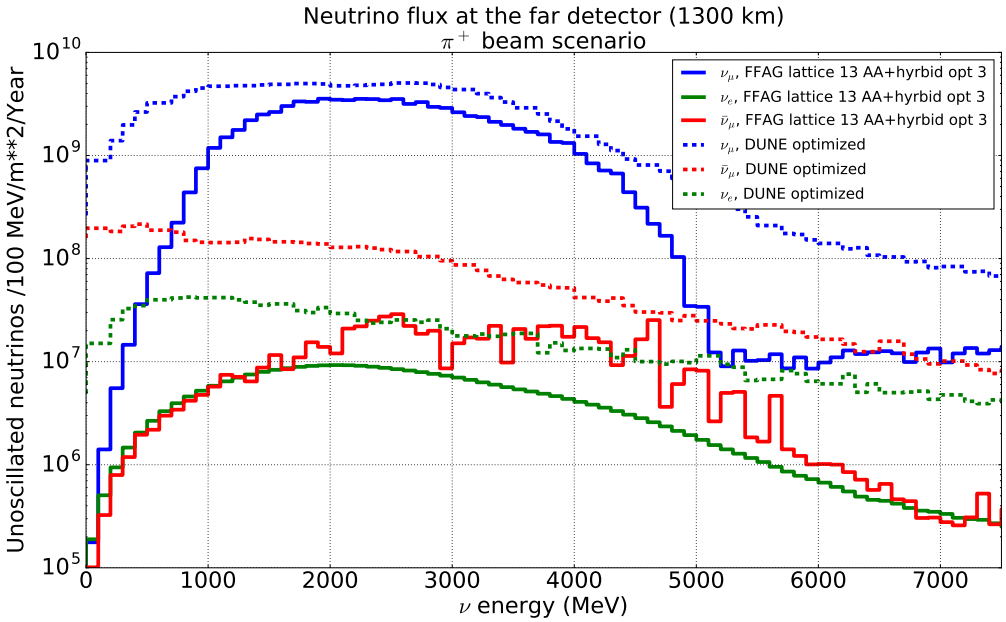

Figure 27. Neutrino fluxes for the optimized 3-horn 62.5 GeV LBNF beam and the nuPIL Lattice 13-hybrid beam (including all backgrounds.)

C. Computing Sensitivities

A sensitivity comparison as was done for the initial study has been repeated (results preliminary) comparing the new nuPIL flux to the LBNF 3-horn optimized flux. The underlying assumptions remain the same, only the fluxes have changed.

1. Sensitivity comparison - Elizabeth Worcester

Unless otherwise noted, all configurations (GLoBES code, oscillation parameters, systematic uncertainties, selection efficiencies, etc.) are identical to those used in the DUNE CDR. There are two LBNF fluxes used in this section. The first is "LBNF optimized" which is a

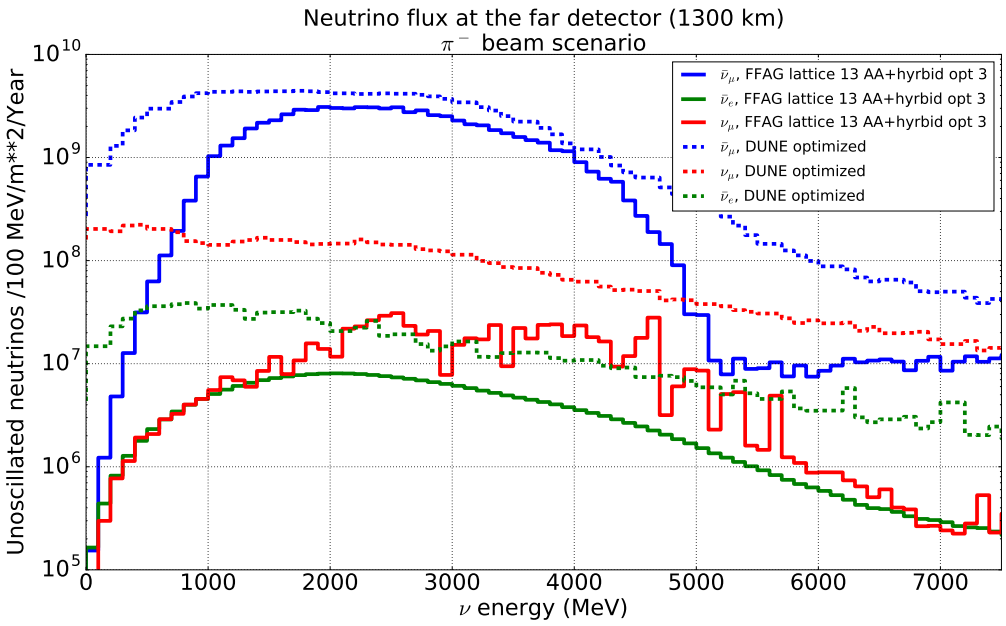

Figure 28. Anti-Neutrino fluxes for the optimized 62.5 GeV 3-horn LBNF beam and the nuPIL Lattice 13-hybrid beam (including all backgrounds.)

flux derived from the CDR parameter set with the exception that the flux here uses a 204 m long decay pipe, whereas the CDR used a 250 m long decay pipe. The second is "LBNF 3-horn optimized" which is the updated LBNF design with 3 horns. The nuPIL flux is the "Lattice 13 with Quad channel" design as used in the previous section.

Since each optimization prefers a different beam energy and the number of POT/year provided by the FNAL complex varies with beam energy, we must compare event rates and spectra assuming equal run time, corresponding to the following POT:

1. LBNF optimized: 80 GeV = 14.7×10^{20} POT/year.
2. LBNF 3 horn: 62 GeV = 18.3×10^{20} POT/year.
3. nuPIL: 80 GeV = 14.7×10^{20} POT/year.

The sensitivity for the mass hierarchy and the CP phase are given in Figures 29 and 30, respectively, where curves for the two LBNF fluxes and the nuPIL flux are given. The curves shown in this figure assume and 7 years of running equally divided between neutrino and antineutrino. In Figure 31, we show the effect that systematic uncertainties have on the CP violation sensitivity. In order the enhance the effect, the exposure was increased to

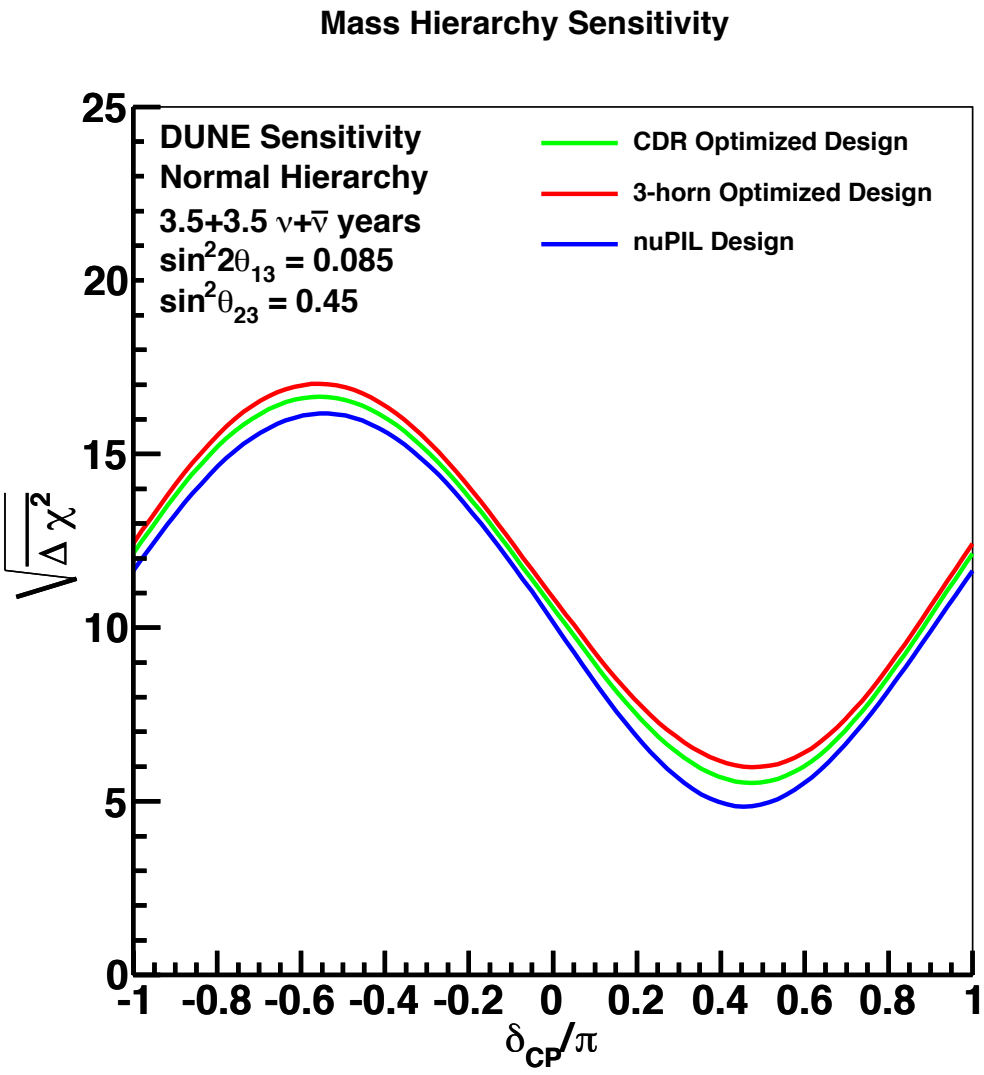

Figure 29. Mass hierarchy sensitivity assuming 7 years of running split equally between neutrino and anti-neutrino.

20.8 years, again equally divided between neutrino and antineutrino running. The nominal systematic uncertainty (solid lines) assumes a 2% uncertainty for the appearance signal and 5% for the disappearance signal. With the nuPIL Lattice13 with Quad channel production straight, a refined estimate of these uncertainties has been made (based on beam line instrumentation and previous studies) giving a somewhat better benchmark of 1.5% uncertainty for the appearance signal and 4.5% for the disappearance signal. These data are indicated in Figure 31 by the dotted line.

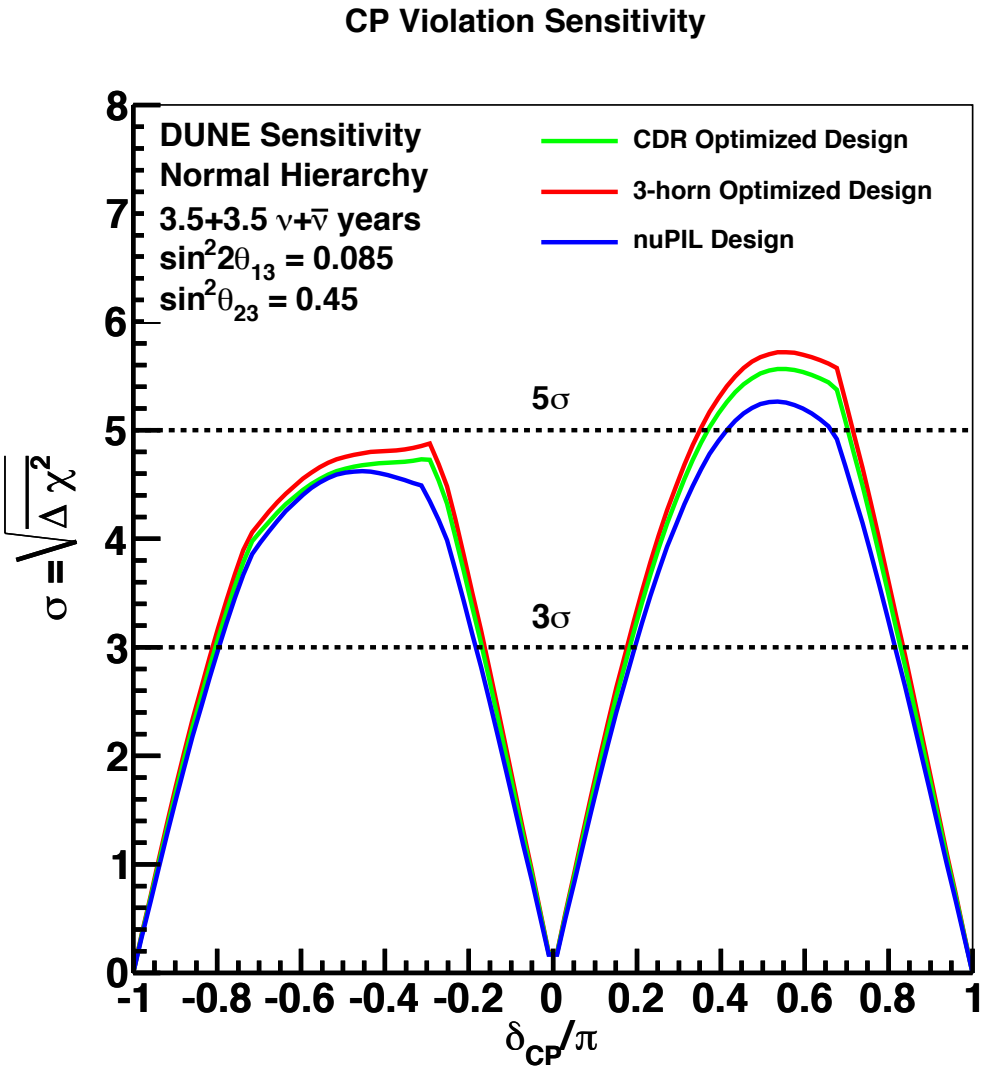

Figure 30. CP phase sensitivity comparison.

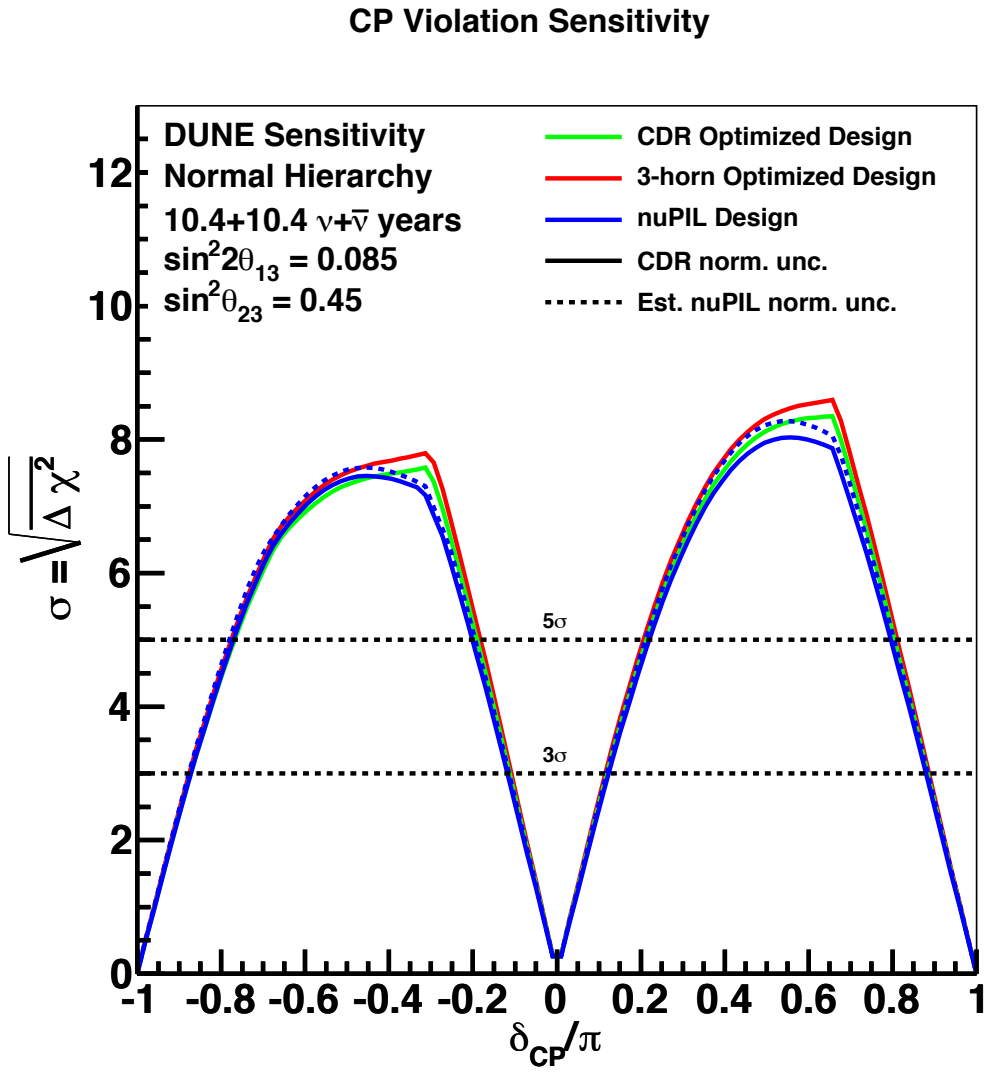

Figure 31. CP phase sensitivity for a large exposure for the baseline normalization uncertainty of $5 \oplus 2\%$ and for an improved estimate uncertainty for nuPIL of $4.5 \oplus 1.5\%$.

V. ENGINEERING CONSIDERATIONS

The nuPIL configuration presents very different engineering considerations with respect to target station design, component lifetime and radiation safety. There are many more active components in the target station for a nuPIL configuration than there are for the conventional LBNF configuration (13 vs. 3), component lifetime, reliability and maintenance therefore becomes a more complicated issue. However, high-power beam exposure is only seen at grade, thus the radiological issues with sending high-power beam underground are eliminated.

A. Target station

The LBNF target station (TS) design currently follows the design of the NuMI target station. However, the NuMI target station design and not accommodate the nuPIL components very easily. A target station as was designed for the first Neutrino Factory (NF) study (US) is a better match to the nuPIL configuration even though in the case of the Neutrino Factory there was no pitch to the beam. Figure 32 presents an overall schematic of the TS that was designed at ORNL for the NF [6]. The Target Support Facility in this design consists of the target region and beam line (decay channel in this NF case), a crane hall over the length of the facility, a maintenance cell at the ground floor elevation for handling magnet components, a hot cell at the tunnel level for the target system components, and various remote-handling equipment used for maintenance tasks. This TS contains water-cooled shielding to limit radiation dose and neutron heating to magnet coils, biological shielding to protect personnel and the environment, and a 50-ton crane that is used for the initial assembly and installation of major components and for subsequent maintenance activities. The target support facility is 12 m wide, and approximately 40 m long. A section view of this TS concept is shown in Figure 33

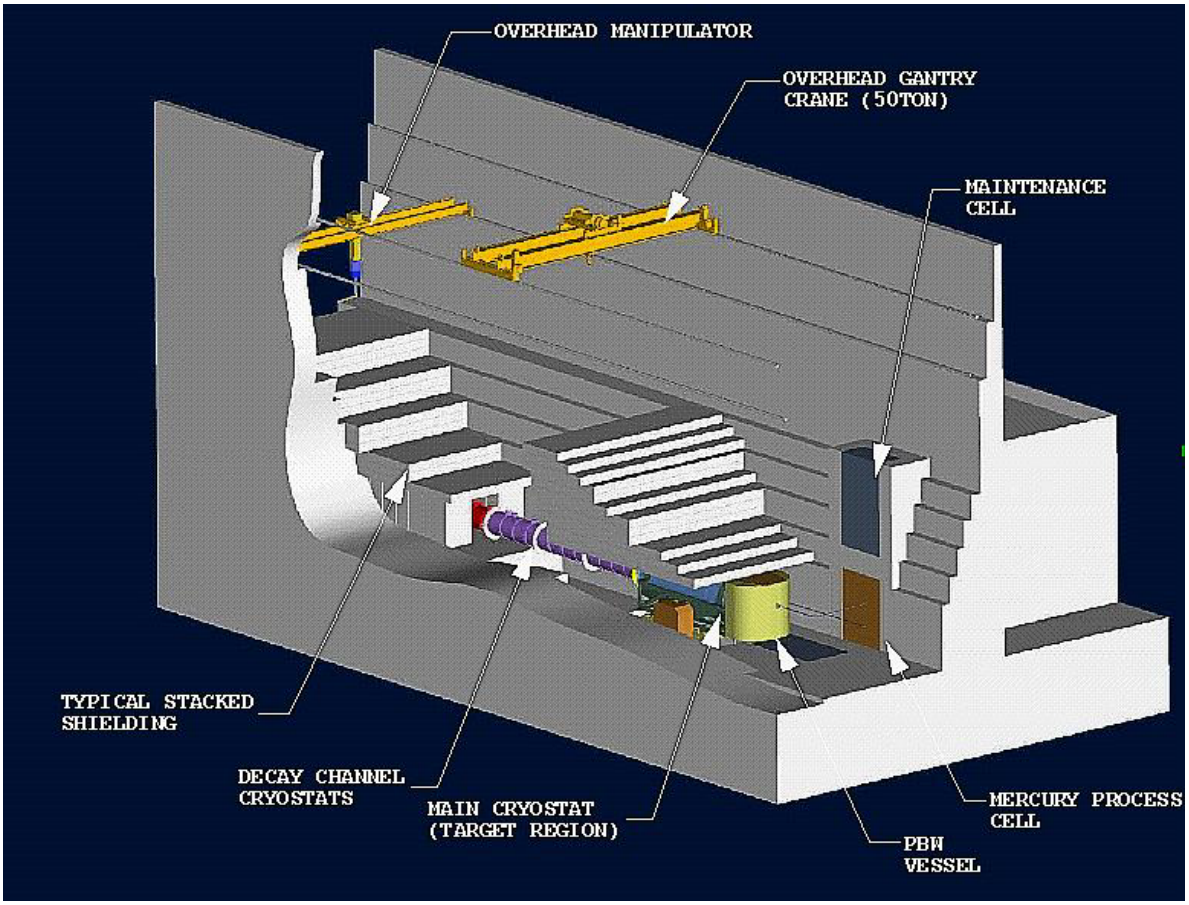

Figure 32. Schematic of TS for NF Design Study I that has features that would support the nuPIL configuration.

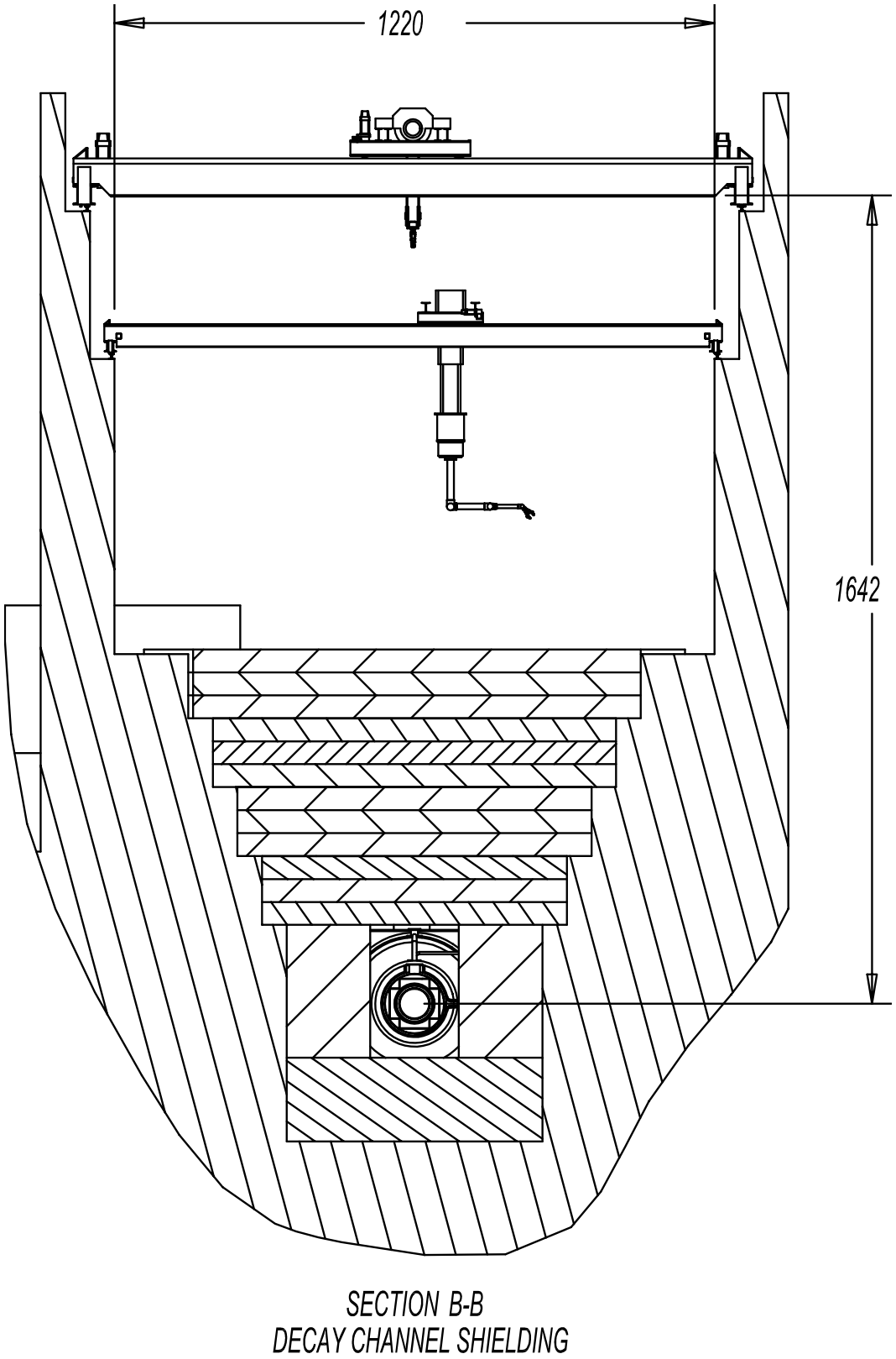

Figure 33. Section view of NF target station design

B. MARS simulation

In order to get a preliminary estimate on the radiation dose to the nuPIL magnets in the bend, a simple MARS model was assembled. In this model a 160 cm long C target is assumed with an 80 GeV proton beam. Cylindrical symmetry was used in order to simply this first pass where the magnets were modeled with an 80 cm cylindrical bore and 1 m thick steel annulus outside the bore to represent the return iron. A constant magnetic field (B=$\pm$0.8T) is imposed in the magnet bores with the direction alternating between adjacent magnets. A the back end of the model is an annulus of polyethylene (outside beam volume) which is a test volume to determine how much radiation might leak out the back of the TS. The MARS model is shown in Figure 34. In Figure 35 the target material was set to vacuum and 5 GeV pions were injected. The figure shows the trajectories of 10 overlapping tracks. Total deposited energy (GeV/g-POT) is shown in Figure 36. The highest dose is seen in the bore (coils) of magnet 1. Utilization of the technology developed for the J-PARC magnets for the neutrino beam line [7] (MgO insulation), we would expect magnet 1 to have a 20 year lifetime at a beam power of 2.4 MW.

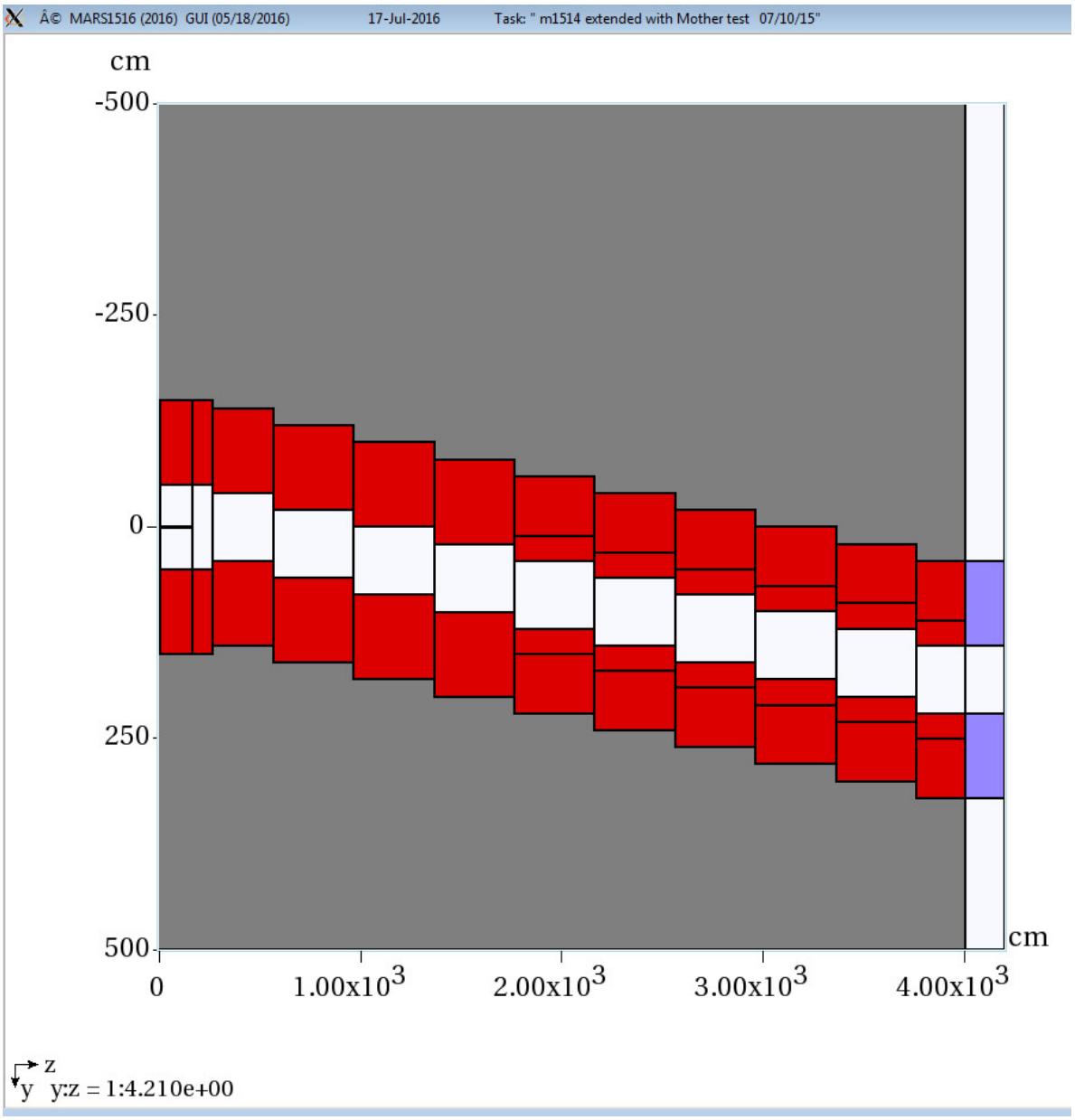

Figure 34. Model used in the MARS simulation: white is vacuum, red is iron, grey is concrete and purple is polyethylene

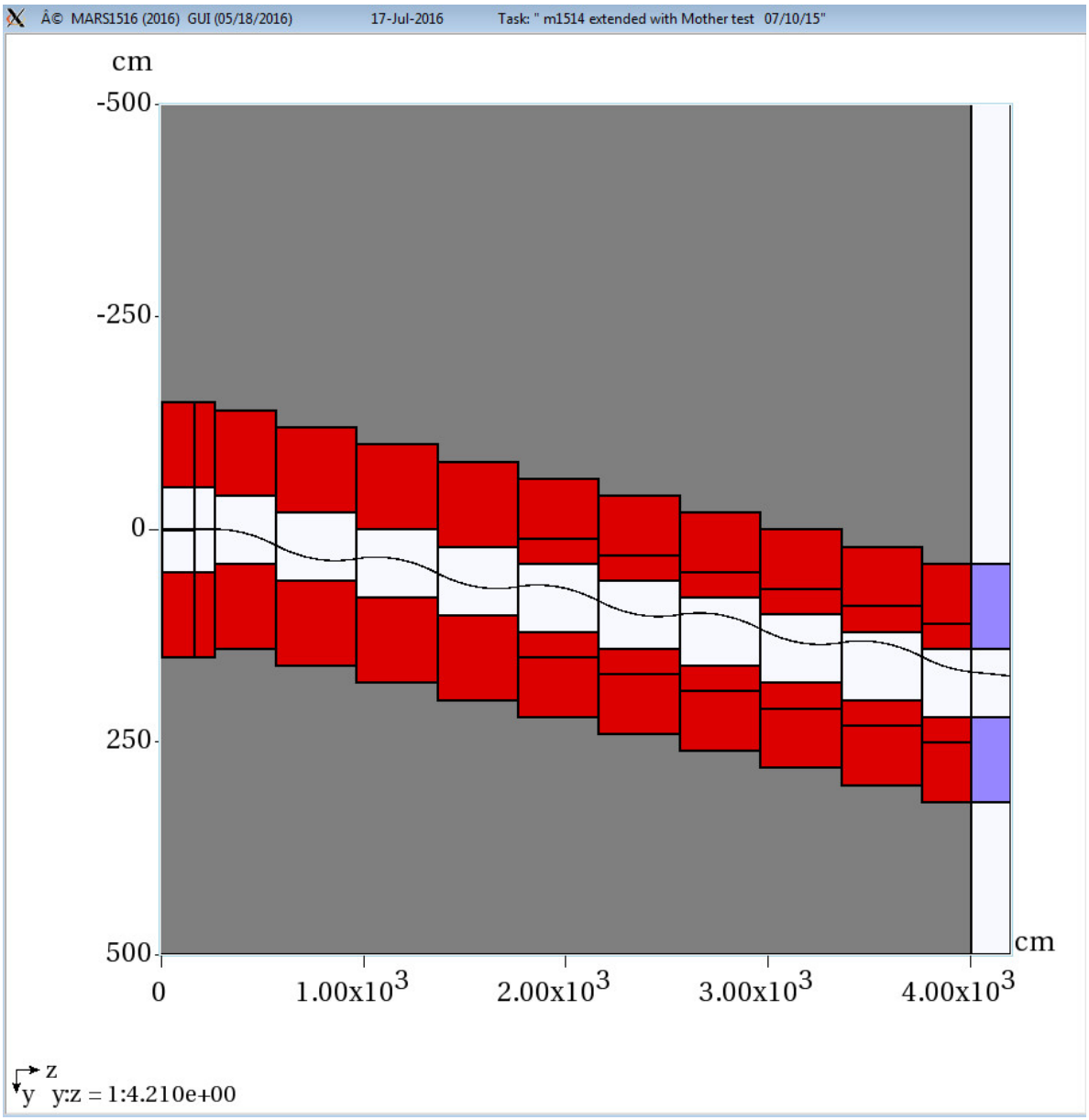

Figure 35. 5 GeV pion tracks (target set to vacuum)

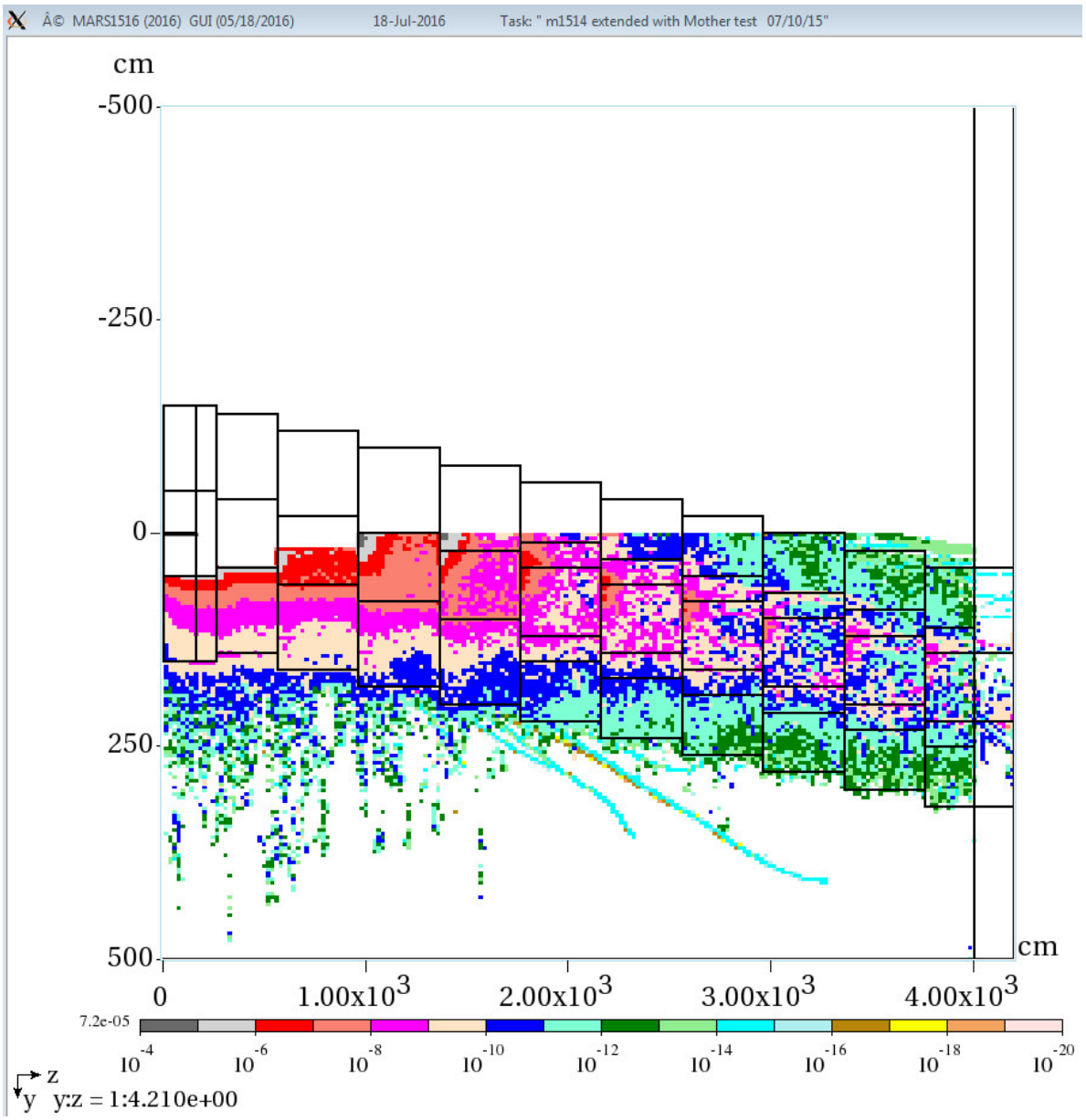

Figure 36. Energy deposition for 80 GeV protons on C. Scale is in GeV/g-POT

VI. ANALYSIS SUITE OVERVIEW

In order to fully understand the physics potential of a nuPIL configuration, physics comparisons will include the basic long-baseline measurements as well as well as rate comparisons at the near-detector site. Some preliminary evaluations of the differences that the two beams may present with respect to physics beyond the νSM will also be given.

A. Beam systematics

Some of the comparisons in Section VI B will be done for beam normalization uncertainties in the two configurations where these uncertainties are twice as large as anticipated. In addition, a comparison will be made in which the near-far flux extrapolation uncertainty is twice what has been calculated. Beam systematics for nuPIL are very different (almost orthogonal) to those in a conventional neutrino beam. In a nuPIL configuration with beam line elements in the straight, the precision of the flux estimates is affected by a number of factors, including: understanding and stability of the magnetic lattice; the overall flux of and type of particles transported by the lattice; and the momentum distributions of those particles. Given the time structure of the beam and the bunch intensity, in the absence of particle decays, beam-current transformers can measure the intensity in the production straight to a precision approaching 0.1%. Determining, quantitatively, the effects of particle decays on the BCTs is work that still needs to be done and is considered an R&D task. In order to investigate the effect of a measurement error on the divergence of the beam, the effect of a mis-measurement/determination of the beam line emittance of the muons stored in the nuSTORM ring was done [1], the muon divergence of each particle in the muon beam was inflated by 2% and the resulting flux compared to the nominal divergence. The statistics-weighted fractional difference between these beams is shown in Figure VI A. The mean difference in the flux in 50 MeV energy bins based on a 2% error in the divergence of the primary beam was determined to be $\simeq 0.6\%$.

Table V. Flux uncertainties expected extrapolated from analyses done for nuSTORM.

Parameter	Uncertainty
Intensity	0.3%
Divergence	0.6%
Energy spread	0.1%
Total	$\lesssim$1%

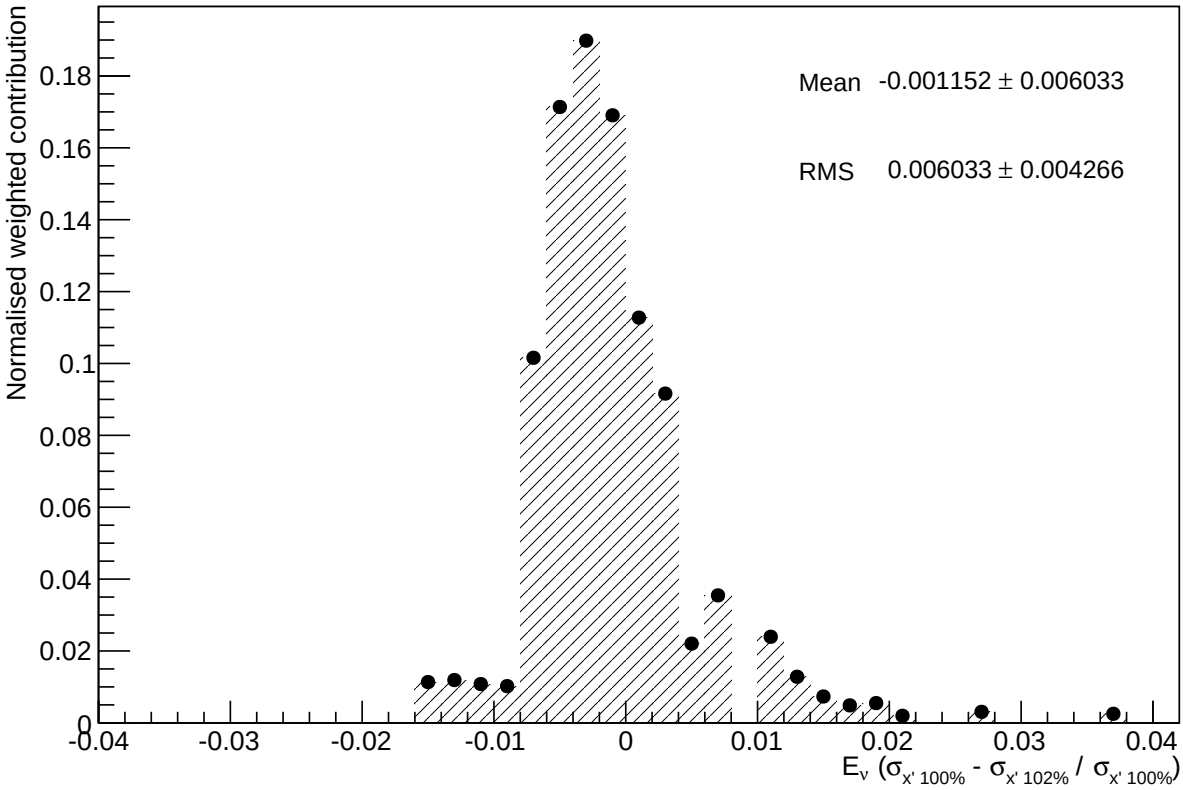

Figure 37. Flux error from divergence/emittance error.

B. Far site

Long-baseline physics comparisons will include:

1. Mass hierarchy
2. CP coverage
3. CP sensitivity as a function of exposure for 75% CP coverage
4. δ_{CP} resolution as a function of exposure
5. θ_{23} resolution

C. Near site

D. Hypotheticals

Some hypotheticals regarding detector performance will also be study. A comparison of the CP reach of the conventional LBNF flux to that of nuPIL will be done for the following hypotheticals:

1. NC background is 4%
2. The missing energy uncertainty is 50%

E. Physics beyond the νSM

??:

1. NSI
2. Steriles
3. DM
4. τ appearance

VII. CONCLUSIONS

[1] D. Adey, R. Bayes, A. Bross, and P. Snopok, Ann. Rev. Nucl. Part. Sci. **65**, 145 (2015).

[2] A. D. Bross, A. Liu, J.-B. Lagrange, and J. Pasternak, PoS **EPS-HEP2015**, 065 (2015).

[3] F. Meot, Nucl. Instrum. Meth. **A767**, 112 (2014).

[4] J. B. Lagrange, T. Planche, E. Yamakawa, T. Uesugi, Y. Ishi, Y. Kuriyama, B. Qin, K. Okabe, and Y. Mori, Nucl. Instrum. Meth. **A691**, 55 (2012).

[5] E. Christensen, P. Coloma, and P. Huber, Phys. Rev. Lett. **111**, 061803 (2013), 1301.7727.

[6] P. Spampinato et al., Tech. Rep. (2001), oRNL/TM-2001/124.

[7] E. Hirose et al., IEEE Trans. Appl. Supercond. **22**, 4101404 (2012).